THE PROPERTIES OF BARRED DISKS IN A SUPERCLUSTER ENVIRONMENT: CONSTRAINTS FROM ABELL 901/2 WITH STAGES

Irina Marinova[1], Shardha Jogee[1], Amanda Heiderman[1], David Bacon[9], Michael Balogh[10], Marco Barden[11], Fabio D. Barazza[4], Eric F. Bell[6], Asmus Böhm[12], John A.R. Caldwell[18], Meghan E. Gray[3], Boris Häussler[3], Catherine Heymans[2,5], Knud Jahnke[6], Eelco van Kampen[11], Kyle Lane[3], Daniel H. McIntosh[15,19], Klaus Meisenheimer[6], Chien Y. Peng[7,8], Sebastian F. Sánchez[13], Rachel Somerville[6], Andy Taylor[14], Lutz Wisotzki[12], Christian Wolf[16], & Xianzhong Zheng[17]
marinova@astro.as.utexas.edu, sj@astro.as.utexas.edu
Draft version August 12, 2008

ABSTRACT

To study bar and host disk evolution in a dense cluster environment, we present a study of ~ 800 bright ($M_V \leq -18$) galaxies in the Abell 901/2 supercluster at z ~ 0.165. We use *HST* ACS F606W imaging from the STAGES survey, and data from *Spitzer*, *XMM − Newton*, and COMBO-17. We identify and characterize bars through ellipse-fitting and other morphological features (spiral arms, prominence of bulge) through visual classification. Our findings are: (1) To define the optical fraction of barred disk galaxies, we explore 3 methods of selecting moderately inclined ($i < 60°$) disk galaxies. We find 350, 256, and 199 such systems, respectively, via visual classification, a Sérsic cut ($n \leq 2.5$), and a blue-cloud cut. These last two methods miss 36% and 50% of visually-identified disks, respectively, especially the many red, bulge-dominated disk galaxies prevalent in clusters. (2) Nonetheless, the three methods of disk selection yield a similar global optical bar fraction ($f_{\rm bar-opt}$) of $\sim 33\% \pm 8\%$ (115/350), $29\% \pm 8\%$ (58/199), and $28\% \pm 8\%$ (72/256), respectively. (3) We explore $f_{\rm bar-opt}$ as a function of host galaxy properties and find that it rises in brighter galaxies and those which are less bulge-dominated. Within a given M_V bin, $f_{\rm bar-opt}$ is higher in visually-selected disk galaxies that have no bulge as opposed to those with bulges. Conversely, for a given visual morphological class, $f_{\rm bar-opt}$ rises at higher luminosities. Both results are similar to trends found in the field. (4) We find no significant trend of $f_{\rm bar-opt}$ with local environment density tracers such as κ, Σ_{10}, ICM density, and projected distance to the nearest cluster center. (5) Furthermore, the cluster optical bar fraction is similar within $\pm 10\%$ to the published field values for bright nearby galaxies, for SDSS early Hubble type systems and faint, disk-dominated galaxies. Our results suggest that the optical bar fraction is not a strong function of local environment.

1. INTRODUCTION

Stellar bars are one of the most important internal drivers of disk galaxy evolution. For field galaxies in the local universe, bars are known to be the most efficient way to redistribute material in the galaxy disk (Combes & Sanders 1981; Weinberg 1985; Debattista & Sellwood 1998, 2000; Athanassoula 2002). Bars channel gas into the central regions of galaxies, where powerful starbursts can ignite (Schwarz 1981; Shlosman, Frank, & Begelman 1989; Kormendy & Kennicutt 2004; Jogee 1999; Jogee, Scoville,

---

[1] Department of Astronomy, University of Texas at Austin, Austin, TX
[2] Department of Physics and Astronomy, University of British Columbia, Vancouver, Canada
[3] School of Physics and Astronomy, The University of Nottingham, Nottingham, UK
[4] Laboratoire d'Astrophysique, École Polytechnique Fédéralede Lausanne, Observatoire, Sauverny, Switzerland
[5] Institut d'Astrophysique de Paris, Paris, France
[6] Max-Planck-Institut für Astronomie, Königstuhl 17, Heidelberg, Germany
[7] NRC Herzberg Institute of Astrophysics, Victoria,Canada
[8] Space Telescope Science Institute, Baltimore, MD, USA
[9] Institute of Cosmology and Gravitation, University of Portsmouth, Portsmouth, UK
[10] Department of Physics and Astronomy, University Of Waterloo, Ontario, Canada
[11] Institute for Astro- and Particle Physics, University of Innsbruck, Innsbruck, Austria
[12] Astrophysikalisches Insitut Potsdam, Potsdam, Germany
[13] Centro Hispano Aleman de Calar Alto, Almeria, Spain
[14] The Scottish Universities Physics Alliance, Institute for Astronomy, University of Edinburgh, Edinburgh, UK
[15] Department of Astronomy, University of Massachusetts, Amherst, MA, USA
[16] Department of Astrophysics, University of Oxford, Oxford, UK
[17] Purple Mountain Observatory, National Astronomical Observatories, Chinese Academy of Sciences, Nanjing, China
[18] University of Texas, McDonald Observatory, Fort Davis, TX, USA
[19] Department of Physics, University of Missouri-Kansas City, Kansas City, MO 64110, USA

& Kenney 2005; Sheth et al. 2005), building central disky structures known as 'pseudobulges' (Kormendy 1982; Kormendy 1993; Jogee 1999; Jogee, Scoville, & Kenney 2005; Fisher 2006; Weinzirl et al. 2008).

As early as 1963, de Vaucouleurs used visual classification on photographic plates to find that approximately 30% of nearby galaxies appear strongly barred in the optical band, with the fraction increasing to approximately 60% if very weak bars are considered. Quantitative studies for the optical bar fraction at $z \sim 0$ yield a mean value of 45% to 52% with a typical uncertainty of $\pm 8\%$ from ellipse-fits (Marinova & Jogee 2007, hereafter MJ07; Barazza, Jogee, & Marinova 2008; hereafter BJM08; Aguerri et al. 2008) and $\sim 47\%$ from bulge-disk-bar decomposition (Reese et al. 2007). The lower value from these quantitative methods compared to the 60% value from de Vaucouleurs (1963) stems from the fact that many weak bars (with RC3 class 'AB') are obscured by dust and star formation (SF), caused by the presence of curved shocks/dust lanes (e.g., Athanassoula 1992) on the leading edges of the bar. Many such bars may fail to meet rigorous quantitative criteria for characterizing bars via ellipse-fit or bulge-disk-bar decomposition, but their presence can sometimes be guessed via visual inspection (see MJ07 for detailed discussion). In the near infra-red (NIR), where obscuration by dust and SF is minimized, different quantitative methods, such as ellipse-fit (Menendez-Delmestre et al. 2007; MJ07), bulge-disk-bar decomposition (Weinzirl et al. 2008) and Fourier decomposition (Laurikainen et al. 2004) all yield a NIR bar fraction of $\sim 60\%$ for bright nearby samples.

The above values of the bar fraction at $z \sim 0$ refer to the globally-averaged value over a wide range of Hubble types and luminosities. Several studies have performed more detailed explorations to look at how bars relate to the properties of the host spiral galaxies. Recent studies based on SDSS (BJM08; Aguerri et al. 2008) using ellipse-fits report that the optical bar fraction rises in spiral galaxies which appear to be disk-dominated, quasi-bulgeless, or have a morphology suggestive of a low bulge-to-disk ratio. A similar trend was observed by Odewahn (1996) using visual classes: he found that the optical fraction of strong bars in disk galaxies rises from Sc galaxies towards later-types. Similar results are found in the near-infrared by Weinzirl et al. (2008) using 2D bulge-disk-bar decomposition on nearby bright spiral galaxies.

Recently, studies performed at intermediate redshifts with the Advanced Camera for Surveys (ACS) on the Hubble Space Telescope (HST) have allowed bars to be probed at earlier epochs. Several studies have shown that the optical fraction of strong ($e > 0.4$) or prominent bars is $\sim 30\%$ on average over $z \sim 0.2$ to 1 (Elmegreen et al. 2004; Jogee et al. 2004; Zheng et al. 2005). In particular, Jogee et al. (2004) find that the optical fraction of strong bars does not show an order of magnitude decline, but is fairly constant, varying from 36%±6% over $z \sim 0.2$ to 0.7 to 24%± 4% over $z \sim 0.7$ to 1.0. A much larger study finds a similar variation in the optical fraction of strong bars from 27%±1% to 12%±1% (Sheth et al. 2008). Interpretations differ on whether the observed decline is simply due to systematic effects such as loss of resolution and rising obscuration with redshift (Jogee et al. 2004; MJ07;

BJM08) or whether it reflects an intrinsic decline (Sheth et al. 2008) in the true bar fraction.

While bars have been studied extensively in the field, little is known about the fraction of bars and their properties in dense environments. We can use galaxy clusters as a lab to test our theories of bar formation and evolution. Also, the presence of bars can be used to test galaxy properties in a cluster environment. In particular, what is the relationship between environmental effects in dense clusters and internal drivers of galaxy evolution such as stellar bars? The detailed process of bar formation is not yet known, but simulations suggest that a cold disk, with low velocity dispersion, σ, favors the formation of spontaneous disk instabilities. External triggers, such as tidal interactions can also induce bars in a dynamically cold disk (e.g., Hernquist & Mihos 1995). Thus, cluster processes can have competing effects on bar formation. Frequent tidal interactions can induce stellar bars, however they may also heat the disks and make them less susceptible to bar formation. Dubinski et al. (2008) explored these effects by modeling the interaction of a hundred DM satellites on M31. They found that while the satellites did not have a large heating effect on the disk, encounters close to the galaxy center could produce strong non-axisymmetric instabilities such as stellar bars. However, in dense clusters, disk galaxies that are deprived of their cold gas through ram-pressure stripping may be too dynamically hot to form bars. In the scenario whereby clusters grow by accretion of field galaxies, these processes may have no effect on an already existing bar. Therefore, the fraction of barred galaxies in a cluster depends on the interplay between these effects, on the epoch of bar formation, and on the evolutionary history of clusters.

There have been only a handful of observational studies that have explored the impact of environment on barred disks. Using a uniform sample of 930 galaxies from the Shapley-Ames catalog, where bar classifications were performed through visual inspection of optical images, van den Bergh (2002) found no difference between the bar fraction in the field and in clusters, and therefore concluded that the bar fraction depends solely on host-galaxy properties. It should be noted that for this study, the environment assignments were largely qualitative, made by inspecting the region around the galaxy on the image, and looking at luminosities and radial velocities of surrounding galaxies. Varela et al. (2004) found that the bar fraction is almost twice as high in galaxies that are interacting, compared to isolated galaxies. This study relied on redshifts from the CfA survey to determine whether a galaxy was being perturbed by a close companion, however their morphological bar classifications came from LEDA and NED which have been known to be notoriously inhomogeneous. The results of Varela et al. (2004) confirm previous studies (e.g., Kumai 1986; Elmegreen et al. 1990; Giuricin et al. 1993), who find a higher number of barred galaxies in binary systems. Recently, Mendez-Abreu, Aguerri, & Corsini (2008) studied the effects of environment on barred galaxies using ~ 3000 galaxies at $0.01 \leq z \leq 0.04$ from SDSS-DR5, and found that the bar fraction and properties were not correlated to galaxy environment. Bars were identified using ellipse fits. However, they excluded interacting galaxies from their study. Barazza et al. (2008, sub-

mitted) study the impact of environment on disk galaxies using ~ 2000 galaxies at intermediate redshift (z $= 0.4-1$) from the EDisCS project.

We are now in a position to make further progress in this largely unexplored aspect of galaxy evolution with the STAGES panchromatic dataset (§ 2), which includes: a 5 × 5 square degree HST ACS mosaic in F606W of the A901/2 supercluster, spectrophotometric redshifts from COMBO-17, coverage with $XMM - Newton$, $GALEX$, and $Spitzer$, as well as dark matter maps. In § 3 we outline the techniques for characterizing bars and disks. It should be noted that traditionally the bar fraction $f_{\rm bar-opt}$ is defined as the fraction of *disk galaxies* that are barred. Hence calculation of $f_{\rm bar-opt}$ requires disk galaxies to be reliably identified. In this paper, we draw attention to the fact that many automated methods commonly used to identify disks in the field may fail in clusters. Motivated by this, we explore different ways of identifying disks (e.g., color cut, Sérsic cut, visual classification, § 4.1) and explore the effect on $f_{\rm bar-opt}$. We explore the frequency of bars as a function of host disk properties (§ 4.3, 4.4, 4.5), and as a function of cluster radius, galaxy number density, ICM density, and DM density (§ 4.6). The comparison of our results to those from field studies is given in § 4.7. We also explore the SF properties of barred and unbarred disks (§ 5). In § 6 we give the summary and conclusions.

2. DATA AND SAMPLE SELECTION

The Abell 901/902 supercluster consists of three galaxy clusters and a group at z ~ 0.165, with an average separation of 1 Mpc. The properties of this system are described in detail in Gray et al. (2002). The STAGES survey (Gray et al. 2008) covers a 0.5 × 0.5 square degree field centered on the supercluster, consisting of an 80-tile mosaic with the HST ACS F606W. The ACS point spread function (PSF) of $0.1''$ corresponds to ~ 282 pc at z ~ 0.165[20]. Spectrophotometric redshifts are available for all galaxies from COMBO-17 (Wolf et al. 2004; 2005) with $\delta z/(1+z) \sim 0.02$ to $R_{\rm Vega} = 24$. The multi-wavelength dataset includes X-ray maps of the ICM density from $XMM - Newton$, UV from $GALEX$, $Spitzer$ 24μ coverage, and dark matter maps from weak lensing (Heymans et al. 2008). Total star formation rates (SFRs) derived from UV and $Spitzer$ 24μ luminosities (Bell et al. 2005), as well as stellar masses (Borch et al. 2006) are also available for this field.

Cluster galaxies are selected using photometric redshifts (see Gray et al. 2008 for a detailed description). This provides a sample of 1990 cluster galaxies. For this paper, we focus on galaxies brighter than $M_{\rm V} \leq -18$. We choose this cutoff, because it tends to separate well the regimes where normal and dwarf galaxies dominate on the luminosity functions of clusters (Binggeli, Sandage, & Tammann 1988). We do not consider dwarf galaxies in this study for two reasons. First, our resolution of ~ 282 pc may be insufficient in many cases to reliably identify morphological structures such as bars in smaller dwarf galaxies. Second, the contamination of the sample by field galaxies at magnitudes fainter than $M_{\rm V} > -18$ becomes significant. This leaves us with a sample of 786 bright ($M_{\rm V} \leq -18$), cluster galaxies.

3. METHODOLOGY

3.1. *Characterization of Bars*

We use the standard IRAF task 'ellipse' to fit ellipses to the galaxy isophotes out to $a_{\rm max}$, where $a_{\rm max}$ is the radius at which the surface brightness reaches sky level. This method of ellipse fitting has been widely used to identify and characterize bars (e.g., Wozniak et al. 1995; Friedli et al. 1996; Regan et al. 1997; Jogee et al. 1999, 2002a, 2002b, 2004; Knapen et al. 2000; Laine et al. 2002; Sheth et al. 2003; Elmegreen et al. 2004; MJ07; Menéndez-Delmestre et al. 2007). We employ an iterative adaptive wrapper, developed by Jogee et al. (2004), which runs the task 'ellipse' up to a maximum number of N iterations. Each iteration uses the previous fit to produce an improved guess for the isophote parameters. N is typically set to 300, but for most objects we obtain a good fit in only a few iterations. A good fit is one where an ellipse is able to be fitted at every radial increment out to $a_{\rm max}$. As described in detail in MJ07, the goodness of the ellipse fits is characterized by the harmonic amplitudes A3, B3, A4, and B4. The amplitudes of these components signify how well the shape of the actual isophote is approximated by the fitted ellipses (e.g., Jedrzejewski 1987). For this sample, we find typical amplitudes of 0–15% in the bar region. We were able to successfully fit 762/786 (97%) of galaxies in our bright cluster sample. The galaxies where 'ellipse' fails generally do not have a regularly decreasing surface brightness profile, which is necessary to define the center for the fitting routine.

We overlay the fitted ellipses onto the galaxy images and plot the radial profiles of surface brightness (SB), ellipticity (e), and position angle (PA). We use both the overlays and radial profiles to classify the galaxies as 'inclined', 'unbarred', or 'barred' using an interactive classification tool developed by Jogee et al. (2004). Galaxies classified as 'inclined' have an outermost isophote with $e > 0.5$, corresponding to $i > 60°$. Because it is difficult to identify morphological structures in such highly inclined galaxies, we do not attempt to classify them as 'barred' or 'unbarred'. For galaxies with moderate inclinations ($i < 60°$), we classify a galaxy as barred if: (1) the e rises smoothly to a global maximum, $e_{\rm bar} > 0.25$, while the PA remains relatively constant (within $\sim 20°$) and (2) the e then drops by at least 0.1 and the PA changes at the transition between the bar and disk region. These criteria have been shown to work well in identifying barred galaxies (e.g., Knapen et al. 2000; Jogee et al. 2002a,b, 2004; Laine et al. 2002). After discarding highly inclined galaxies (230 or 30%) and those with visually-identified poor fits (57 or 7%), we are left with 475 moderately inclined ($i < 60°$), bright ($M_{\rm V} \leq -18$) cluster galaxies. Note that this number includes *all* moderately inclined, bright galaxies and not just disk galaxies, as ellipse-fitting was performed on the whole sample.

The luminosity and color distributions of the total fitted sample of 762 bright, cluster galaxies and the moderately inclined sample of 475 galaxies are over-plotted in Figure 1(a) and (b), respectively. An example of the overlays and radial profiles of a barred cluster galaxy are shown in Figure 2. Because we are looking at optical wavelengths,

---

[20] We assume in this paper a flat cosmology with $\Omega_M = 1 - \Omega_\Lambda = 0.3$ and $H_0 = 70$ km s^{-1} Mpc^{-1}.

in rare cases the criterion of constant PA in the bar region may not be satisfied. This can happen in galaxies where the bar is weak, and the dust lanes along the leading edges of the bar are curved, producing a 'twisting' in the PA radial profile (Athanassoula 1992b). We find 37 such cases (8%), which we classify as 'unbarred' because they do not satisfy the constant PA criterion. The advantages and limitations of the ellipse-fitting method are further discussed in detail in MJ07.

In addition to quantitatively identifying and characterizing bars using ellipse fitting, we also visually classify all galaxies in the sample. The identification of bars through visual inspection provides an independent check for the detection of bars through ellipse-fits. The visual bar classification agrees with the ellipse fits for over 90% of cases. For the cases where a bar is found through visual classification, but not through ellipse-fitting, it is because dust and gas mask the bar signature, making the PA twist. We conservatively take the error in the optical bar fraction as the sum in quadrature of the binomial term and the error of 8% caused by isophotal twists. Representative barred galaxies from the cluster sample are shown in Figure 3.

3.2. *Methods for Selection of Disk Galaxies*

In all studies conducted to date (e.g., deVaucouleurs 1963; Sellwood & Wilkinson 1993; Eskridge et al. 2000; Knapen et al. 2000; Mulchaey & Regan 1997; Jogee et al. 2004; Laurikainen et al. 2004; Elmegreen et al. 2004; Zheng et al. 2005; Buta et al. 2005; MJ07; Menéndez-Delmestre et al. 2007; BJM08; Sheth et al. 2008), the bar fraction, $f_{\mathrm{bar-opt}}$ has been defined as the number of barred *disk* galaxies divided by the total number of *disk* galaxies:

$$f_{\mathrm{bar-opt}} = \frac{N_{\mathrm{barred}}}{N_{\mathrm{disk}}} = \frac{N_{\mathrm{barred}}}{N_{\mathrm{barred}} + N_{\mathrm{unbarred}}}. \quad (1)$$

Note that in the above studies, as well as in this paper, we use the term 'disk galaxies' to describe all galaxies with a disk component (e.g., S0-Sm), which may or may not be accompanied by a bulge. The bar fraction is only quoted with disk galaxies in mind, because bars are believed to be an $m = 2$ instability in the disk component of galaxies. Also, if the bar fraction were calculated over *all* galaxies, changes in the morphological distribution between disk and spheroidal galaxies would influence the bar fraction and make it hard to compare across different samples. In the local universe, for nearby galaxies, catalogs like the RC3 (deVaucouleurs et al. 1991) contain visual classifications of galaxy morphology, making it possible to select a sample of disk galaxies for bar studies. In large surveys such as the SDSS and GEMS, two quantitative methods have been used to pick out disk galaxies: (1) using a blue-cloud color cut in color-magnitude space (Jogee et al. 2004; BJM08) and (2) using a Sérsic index, n, from a single component fit to select disks (Jogee et al. 2004; Barden et al. 2005; Ravindranath et al. 2004). In the color cut method, only blue cloud galaxies are selected on a color-magnitude diagram. The Sérsic cut method involves selecting only galaxies with Sérsic index $n < 2.5$. This is motivated by the fact that a pure disk has a Sérsic index of 1, while a deVaucouleurs profile typically used to describe a spheroid has a Sérsic index of 4. Inspection of a visually selected sample (e.g., Bell et al. 2004; Jogee et

al. 2004; McIntosh et al. 2005) has shown that $n \leq 2.5$ is a good dividing line in separating disk galaxies from spheroids. In fact, most disk galaxies have Sérsic index $n < 3$ (Weinzirl et al. 2008), although the scatter is large within a given Hubble Type.

Using a blue-cloud or Sérsic cut to pick out disk galaxies works fairly well in the field. However, these methods can fail in a cluster environment, where the galaxy populations are different than those in the field. Gas stripping of spirals could quench their star formation and make them look redder. These galaxies might then be missed by a color cut. On the other hand, the prevalence of bulge-dominated S0-type disk galaxies in clusters (Dressler 1980) could be missed by a Sérsic cut. For this reason, we use a third method to pick out disk galaxies: visual classification.

We visually classify the whole sample and put galaxies into different groups according to the galaxy morphology (§ 3.3). A galaxy is identified as a disk galaxy if it exhibits the dynamical signatures of disk instabilities such as a stellar bar and spiral arms. In the absence of such structure, disks are picked by an identifiable break between the bulge and disk component either in the image itself and/or using an estimation of the brightness profile with the Smithsonian Astrophysical Observatory visualization tool *DS9*. Three classifiers (I.M., A.H.,S.J.) completed a training set of several hundred galaxies, and two classifiers (A.H., I.M.) classified the full cluster sample, with the third classifier performing random checks. Subsequently, uncertain cases were reviewed by all three classifiers. In our fitted sample of 762 galaxies, 744 of them could be classified into the visual classes described above. The remaining galaxies were either too messy to classify, too compact to classify, or unclassifiable for other reasons, such as noise or edge effects. We could not reach agreement on 4% of cases regarding whether a galaxy was a pure bulge or contained a disk component. Results from the different methods of disk selection are presented in § 4.1.

3.3. *Visual Classification of Secondary Morphological Parameters*

For our cluster sample, we visually classify secondary morphological parameters such as the prominence of the bulge and the presence of gas and dust.

Because we are only interested in studying large-scale bars that extend well beyond the bulge region of the galaxy, the prominence of the bulge is not key for determining the bar fraction. It is interesting, however, for studying and interpreting correlations between bar and host disk properties (see § 4.3–4.5). Our goal is not to finely measure the bulge-to-total light (B/T) ratio in galaxies, but to identify galaxies with extreme B/T, such as systems that appear nearly bulgeless and likely have very low B/T, and those with prominent bulges, suggestive of high B/T. We thus classify galaxies into three broad groups: 'pure bulge'(Fig. 4a,b), 'pure disk' (Fig. 4g–j), and 'bulge+disk' (Fig. 4c–f). 'Pure disk' galaxies are those where no central spheroidal component is seen. Conversely, a galaxy is classified as a 'pure bulge' if its morphology is spheroidal and there is no break in the brightness profile, indicative of the transition between the bulge-dominated and disk-dominated region. In addition, 'pure

bulge' galaxies do not exhibit disk features such as spiral arms or stellar bars. In our cluster sample of bright galaxies, we find that 23% ± 13% of galaxies are visually classified as 'pure disk', 60% ± 12% are classified as 'bulge+disk', and 17% ± 1% were classified as 'pure bulge.' These results are summarized in Table 3. The values quoted are from the averaged classifications of A.H. and I.M. and the percent errors indicate the sum in quadrature of the dispersion between classifiers and the binomial term of the statistical error. The disagreement is due to the inherent difficulty in separating ellipticals from disk galaxies, when the disk is smooth and has no unambiguous disk signature, such as a bar or a spiral arm.

We also visually classify galaxies into those with a clumpy or smooth disk, motivated by the following considerations. Firstly, the presence of gas, dust, and star formation along the bar can prevent its detection in optical images, particularly for weak bars. In weak bars the dust lanes are curved because of weaker shocks (Athanassoula 1992). In addition, weaker shocks can induce star formation along the bar, while strong shocks are accompanied by straight dust lanes and tend to suppress star formation along the bar (e.g., Elmegreen 1979; Das & Jog 1995; Laine et al. 1999; Jogee, Scoville, & Kenney 2005). The curved dust lanes and star formation regions in weak bars produce a pattern that causes fitted ellipses to have varying PA along the bar, and to sometimes fail to satisfy the criterion of a flat PA plateau along the bar (§ 3.1). In very gas/dust-rich galaxies, even strong bars can be masked by dust and star formation. These effects make it more difficult to identify bars at optical wavelengths (e.g., Block et al. 1994). Several studies (Laurikainen et al. 2004; MJ07) show that, because of obscuration by gas, dust, and star formation regions in the optical, the bar fraction is higher in the infrared (IR) band by a factor of ∼ 1.3 for galaxies at z ∼ 0. In cluster environments, the correction factor for bar obscuration is unknown.

Secondly, it is useful to explore the relationship between clumpiness, the visual prominence of the bulge (or B/T ratio), and bars in cluster environments, where the situation might well differ from the field. In the field, along the traditional Hubble Sequence, on average the visual prominence of bulge and the tightness of the spiral arms increase from Sd to Sa, while the clumpiness of the spiral arms decreases. In field galaxies, there is a wide range of B/T for each Hubble type, with low B/T galaxies being present across S0 to Sc (Laurikainen et al. 2007; Weinzirl et al. 2008; Graham & Worley 2008), but the average B/T tends to fall in later Hubble types (Laurikainen 2007; Weinzirl et al. 2008; Graham & Worley 2008). In clusters, where a number of processes, such as ram-pressure stripping or galaxy harassment can alter the gas content of galaxies, the relationship between B/T and gas/SF content or clumpiness of the disk may break down. For example, in the Virgo cluster, the central concentration of galaxies does not correlate with their star formation properties, as it does in the field (Koopmann & Kenney 2001).

Motivated by these considerations, we attempt to visually characterize the presence of gas and dust in galaxies (see Table 3). The degree of 'clumpiness' in a galaxy is used as a rough proxy for estimation of the presence of gas and dust. We allocate galaxies into two broad classes:

(1) 'smooth' galaxies that show no patchy obscuration by gas and dust or (2) 'clumpy' galaxies with gas and dust. We find that 74% ± 9% (551/744) of the bright galaxies in our supercluster sample appear mostly smooth (contain little or no gas and dust), while 26% ± 9% (199/744) of the bright galaxies appear clumpy (contain some gas and dust). Examples of 'smooth' galaxies are shown in Fig. 4, panels a–d and i–j. 'Clumpy' galaxies are shown in panels e–h of Figure 4.

4. RESULTS AND DISCUSSION

4.1. *Selection of Disk Galaxies in Clusters*

How well do the Sérsic and blue-cloud cut methods pick out disk galaxies when compared to visual classification? Our moderately inclined (i < 60°), bright sample ($M_{\rm V}$ ≤ − 18), with good ellipse-fits, totals 475 galaxies. All numbers quoted hereafter are derived from this sample. Out of these, we identify 350 disk galaxies through visual classification (see § 3). Figure 5 compares the disk galaxies identified through three different methods: visual classification, blue-cloud color cut, and a Sérsic cut. Panel (a) shows where the visually identified disk galaxies (filled circles and open squares) lie in the rest-frame $U − V$ vs. $M_{\rm V}$ plane. The systems are further split into disk galaxies with a bar and/or spiral arms (filled circles) and ones without (open squares). The black points represent all other galaxies, not classified as disks. The solid line separates the red sequence from the blue cloud galaxies, using the equation

$$U-V = (1.48-0.4\times0.165-0.08\times(M_{\rm V}+20.0))-0.25, \quad (2)$$

derived for the STAGES sample by Wolf, Gray, & Meisenheimer (2005), where $M_{\rm V}$ is the V absolute magnitude and $U − V$ is the rest-frame color. Panel (b) shows where visually identified disk galaxies lie in the $U − V$ color vs. Sérsic index n plane. Symbols are the same as in panel (a). The solid line shows the cutoff of $n = 2.5$, which is supposed to separate disk galaxies and spheroids.

Identifying disk galaxies as those with a Sérsic index n < 2.5 (Fig. 5b) picks out 64%± 4% (223/350) of galaxies visually selected as disks. The Sérsic cut method will pick up many of the red disks that the color cut misses, however the Sérsic cut method might miss some early-type disk galaxies with very prominent bulges or very clumpy galaxies with bright star formation regions in their outer disks. In addition, the presence of an AGN will drive the Sérsic index to high values. Figure 6a shows examples of visually-identified disk galaxies missed by the Sérsic cut.

Our analysis suggests that the Sérsic cut misses 36%± 4% of visually-identified disks. How robust is this number? We consider the possibility that some galaxies visually classified as disk galaxies ('pure disk' or 'bulge+disk') may in fact be misclassified ellipticals. This is most likely to happen when the disk is smooth and has no unambiguous disk signature, such as a bar or a spiral arm. As stated in § 3.3, it is difficult to separate a 'pure bulge' galaxy from an unbarred, smooth 'bulge+disk' (e.g., S0) without spiral arms. In addition, unbarred 'pure disk' galaxies without spiral arms that appear mostly smooth could also be misclassified ellipticals. As a firm lower limit to the number of visually-identified disk galaxies missed by the Sérsic cut we consider disk galaxies ('pure disk' or 'bulge+disk') that have a clear disk signature such as a

bar and/or spiral arms. This sets a firm lower limit on the number of disk galaxies that are missed by a Sérsic cut. We find that at least 24% (52/218) of the galaxies with $n > 2.5$ are visually-identified disk galaxies. Thus, in summary, we estimate that 24% to 36% of visually-identified disk galaxies are missed by taking a Sérsic cut ($n < 2.5$).

Selecting blue cloud galaxies only picks out 50%± 4% (178/350) of the visually-identified disk galaxies. The 172 galaxies missed are on the red sequence and the large number of these galaxies is consistent with the high number of red disks in a cluster environment. Figure 6b shows some examples of visually-identified disk galaxies on the red sequence, which would be missed if a blue-cloud color cut is used to pick out disks.

We can look at the composition of the red sequence in more detail. The 172 visually-identified disks make up 63% of the total population of 276 red sequence galaxies. Galaxies classified as 'pure bulge' (e.g., E's) make up 38% (104/276). Out of the galaxies visually identified as disks on the red sequence, 98% (168/172) are classified as 'bulge+disk' and only 2% (4/172) are classified as 'pure disk' with no visible bulge component.

The large proportion of the red sequence consisting of visually identified disk galaxies may seem surprising if one typically thinks of the red sequence as made up mostly of ellipticals. Again, we set a firm lower limit to the disk galaxies on the red sequence, by considering disk galaxies ('pure disk' or 'bulge+disk') that have a clear disk signature such as a bar and/or spiral arms. This gives a robust lower limit of 24% (67/276) of galaxies on the red sequence that are disks ('bulge+disk' or 'pure disk'). Thus, in summary, our results suggest that 24% to 63% of the red sequence is made up of disks, with the large range primarily caused by the difficulty in differentiating red, featureless S0-type galaxies from spheroidals. A significant fraction of dusty, red disk galaxies in the supercluster sample is also found by Wolf et al. (2008, in prep), where the properties of these galaxies are discussed in detail.

Unless otherwise stated, we use the visual classifications to define a disk galaxy sample in the remaining analysis.

4.2. *Global Optical Bar Fraction*

The optical fraction of barred galaxies *among all galaxies* brighter than M_V =-18, is 24%. However, this number is not very useful as changes in this number can reflect a change in the disk fraction, as well as the fraction of disks that host bars. Furthermore, bars are stellar features and $m = 2$ instabilities that occur only in disks, and insights into their formation and evolution can be best gleaned by inspecting the fraction of disks that are barred at different epochs and in different environments.

This has motivated the definition of the bar fraction as the fraction of disks that are barred as given by Equation 1. All studies of bars to date (e.g., deVaucouleurs 1963; Sellwood & Wilkinson 1993; Eskridge et al. 2000; Knapen et al. 2000; Mulchaey & Regan 1997; Jogee et al. 2004, Laurikainen et al. 2004; Elmegreen et al. 2004; Zheng et al. 2005; Buta et al. 2005; MJ07; Menéndez-Delmestre et al. 2007; BJM08; Sheth et al. 2008) have adopted this definition and thus provide complementary comparison points for our studies.

For the STAGES cluster sample, three methods of selecting disks are available: visual classification, blue cloud selection, and Sérsic cut selection. As mentioned in § 3.2 and Eq. 1, it is necessary to identify a sample of disk galaxies N_{disk}, in order to determine the optical bar fraction, $f_{bar-opt}$. Because of the problems in selecting disks in a cluster sample using the quantitative color or Sérsic cuts (see § 3.2 and 4.1), we estimate $f_{bar-opt}$ using visual classification to select disk galaxies. We obtain an optical bar fraction of $f_{bar-opt} = 33\%\pm 8\%$. This value is similar to the optical bar fraction $f_{bar-opt-EDisCS}$ ~25% found for galaxies brighter than $M_V = -19$ in intermediate-redshift (z = 0.4 − 1) clusters by Barazza et al. (2008).

For completeness, we also calculate the bar fraction using a blue-cloud color cut and Sérsic cut to select disk galaxies. The results are shown in Table 1 for bright ($M_V \leq -18$) galaxies, and in Table 2 for galaxies with $M_*/M_\odot > 10^9$. In all cases, regardless of the disk selection method, we obtain an optical bar fraction $f_{bar-opt}$ of 27–33% with a typical error of ± 8%. This result implies that the optical bar fraction in blue galaxies picked out by the color cut and that in low Sérsic index galaxies, is similar to the total average bar fraction found through selecting disk galaxies by visual classification (Table 1). For $M_*/M_\odot > 10^9$ galaxies, similar results are found (Table 2).

4.3. *Optical Bar Fraction as a Function of B/T*

We explore the relationship between the optical bar fraction and host galaxy properties, such as the prominence of the bulge.

The relationship between the bar, bulge, and disk components is an area under active study both theoretically and observationally (e.g., Reese et al. 2007; Laurikainen et al. 2007; Weinzirl et al. 2008; BJM08; Aguerri et al. 2008). In one theoretical scenario, bars can form and be maintained through the swing amplification of gravitational instabilities (e.g., Toomre 1981; Binney & Tremaine 1987). Such bars are less likely to grow in galaxies where a prominent bulge leads to an inner Lindblad resonance (ILR), which cuts off the swing amplification loop. Therefore, in this scenario, it is expected that late-type galaxies with a low B/D ratio are more likely to host bars than bulge-dominated galaxies (e.g., S0/Sa). Some observational evidence to this is provided by results showing a higher optical bar fraction in late-type galaxies with lower central light concentration (BJM08; Aguerri et al. 2008). It is also possible, however, that the gas-rich, dynamically colder disk of late types may also play a part in the higher observed optical bar fraction.

Another relationship between bars and bulges is that some bulges may form via mechanisms tied to the bar. Through the redistribution of disk material, bars can build disky central concentrations known as pseudobulges (Kormendy 1982; Kormendy 1993; Jogee 1999; Athanassoula 2005; Sheth et al. 2005; Jogee, Scoville, & Kenney 2005; Fisher 2006). Interestingly, pseudobulges may also be formed through minor mergers (Weinzirl et al. 2008). Boxy/peanut bulges observed in edge-on galaxies (e.g., Lütticke, Dettmar, & Pohlen 2000; Bureau & Athanassoula 2005) are thought to be the central parts of bars that undergo a process of vertical 'buckling' during their

evolution (Bureau & Freeman 1999; Athanassoula et al. 2005; Debattista et al. 2006; Martinez-Valpuesta et al. 2006) and/or due to a vertical ILR (Combes & Sanders 1981; Combes et al.1990, Sellwood 1993; Kuijken & Merrifield 1995).

While we did not perform a structural bulge+disk+bar decomposition to accurately characterize B/T (e.g., Laurikainen et al. 2007, Weinzirl et al. 2008), we can use the three broad visually-classified groups of galaxies: 'bulge+disk', 'pure disk', and 'pure bulge'.

We plot the optical fraction of bars as a function of morphological class in Figure 7a. Here the morphological classes have been grouped by the visual prominence of the bulge. Galaxies with a 'bulge+disk' component are in the first bin, while 'pure disk' galaxies are in the second bin. We find that $f_{\rm bar-opt}$ increases from 29%± 3% in 'B+D' galaxies to 47%± 6% in 'pure disk' galaxies, suggesting that the optical bar fraction rises in spiral galaxies, which are disk-dominated and have very low bulge-to-disk ratios (Table 3).

This result is further suggested by Figure 7b, which shows the optical bar fraction as a function of central concentration in the host galaxy, as characterized by the effective radius normalized to the disk radius, $r_{\rm e}/a_{disk}$. The effective radius $r_{\rm e}$ is calculated from single-component Sérsic fits (Gray et al. 2008). The disk semi-major axis a_{disk} comes from the semi-major axis of the outermost ellipse fitted to each galaxy, where the isophotes reach sky level (see § 3.1). The optical bar fraction clearly increases with decreasing central concentration, from 15%± 9% in galaxies with high concentration ($r_{\rm e}/a_{disk}$=0.15), to 50%± 12% in galaxies with low concentration ($r_{\rm e}/a_{disk}$=0.75). Note that for this study, we focus on large-scale bars in bright galaxies only, which are defined as having semi-major axis larger than 1 kpc, and which extend significantly past the bulge region. It is therefore very unlikely that this trend is a systematic effect caused by difficulty in identifying bars in galaxies with larger bulges.

The rise in the optical bar fraction as a function of the prominence of the bulge or central concentration of the host galaxy is in agreement with BJM08, who found that the optical bar fraction in pure disk galaxies is a factor of ~ 2 higher than in disk galaxies with prominent bulges, from an SDSS sample of $M_{\rm V} \leq -18.6$ galaxies and redshift range $0.01 \geq z \geq 0.03$. This result is confirmed by Aguerri et al. (2008, in prep), who find that the optical bar fraction increases from 30% in S0 galaxies, to 52% in late-type (Sc-Sd) systems, using SDSS galaxies at $0.01 \geq z \geq 0.04$. Similar results are found by Weinzirl et al. (2008) using 2D bulge-disk-bar decomposition on nearby bright spiral galaxies. For disk galaxies with $M_{\rm B} < -19$, the bar fraction increases from 31%± 13% in spirals with B/T ≥ 0.4, to 68%± 4% in spirals with B/T ≤ 0.2 (see their Table 8 and § 5.6).

4.4. *Optical Bar Fraction as a Function of Host Luminosity*

In Figure 8a-c we show the optical bar fraction as a function of host galaxy rest-frame $M_{\rm V}$ luminosity. The optical bar fraction is calculated for all three methods of disk selection (color cut, Sérsic cut, and visual classification). For all three methods of disk selection, the optical bar fraction

shows a decrease from $\sim 60\%± 10\%$ at $M_{\rm V} = -21.5$ to $\sim 20\%± 8\%$ at $M_{\rm V} = -18.5$.

This result may seem counter-intuitive given the fact that we find a lower optical bar fraction in bulge-dominated galaxies, and we might expect such systems to be on average brighter. In such a case, one might expect that the optical bar fraction falls for brighter disk galaxies. However, Fig 9 explains why we find the opposite result. This figure shows the optical bar fraction in a two-dimensional parameter space defined by morphological class and luminosity. Here the morphological classes refer to the four visually-classified disk morphological classes: 'bulge+disk smooth', 'bulge+disk clumpy', 'pure disk smooth', and 'pure disk clumpy'. Fig. 9 shows that the optical bar fraction is higher at brighter $M_{\rm V}$ *for any given morphological class*. Therefore, when all of the visual morphological classes are grouped together and $f_{\rm bar-opt}$ is calculated as a function of $M_{\rm V}$ in Fig. 8c, the optical bar fraction is higher for brighter magnitudes.

This result is consistent with the findings of Barazza et al. (2008) for cluster galaxies at intermediate redshifts (z = 0.4 − 1). This study also finds that, although brighter, early Hubble type galaxies host less bars than fainter, late-type galaxies, withing a given Hubble Type, brighter galaxies on average have a higher optical bar fraction.

4.5. *Optical Bar Fraction as a Function of Host Color*

We find no significant difference in the optical bar fraction in disks on the red sequence and blue cloud. When disks are selected through visual classification, the optical bar fraction on the red sequence is $f_{\rm bar-RS} \sim 31\%± 3\%$ while on the blue cloud, it is $f_{\rm bar-BC} \sim 32\%± 4\%$. This can be visualized by inspection of Fig. 5. The similar values for the blue cloud and red sequence explain in part why the global optical bar fraction $f_{\rm bar-opt}$ based on visual selection of disks, is similar to the one obtained by selecting disks via a blue cloud cut.

Taking a global average of the optical bar fraction across the blue cloud and red sequence may not reveal the true dependence of the optical bar fraction on color, because the relative number of bright to faint galaxies is different on the blue cloud and red sequence, with the red sequence having more bright galaxies (Fig. 5). The latter have a higher optical bar fraction than fainter galaxies, since the optical bar fraction rises at higher luminosities for each given morphological type (§ 4.4; Fig. 9).

Therefore, we repeat the exploration of the optical bar fraction as a function of color, by looking at the breakdown of the optical bar fraction in the rest-frame $U - V$ vs. $M_{\rm V}$ plane (Fig. 10a), and the rest-frame $U - V$ vs. visual morphological class (bulge+disk vs. pure disk) plane (Fig. 10b). We find that for galaxies fainter than $M_{\rm V} \sim -20$, at given luminosity, the optical bar fraction increases as rest-frame $U - V$ color becomes bluer (Fig. 10a). However, for galaxies brighter than $M_{\rm V} \sim -20$, at given luminosity, the optical bar fraction decreases as rest-frame $U - V$ color becomes bluer (Fig. 10a). Fig. 10b shows that for a given morphological class, the optical bar fraction remains about the same as rest-frame $U - V$ color becomes bluer, however for the class 'bulge+disk smooth', it decreases at bluer colors.

4.6. Optical Bar Fraction as Function of Kappa, Σ_{10}, ICM density, and Distance to Nearest Cluster Center

Bars can act as a tool to probe the evolution of galaxies. Frequent tidal interactions can induce stellar bars in dynamically cold disks (Quinn et al. 1993; Hernquist & Mihos 1995; Mihos et al. 1995; Dubinski et al. 2008). However, they may also drive gas from the disk to the central regions of galaxies, and tidally heat them, making them less bar unstable. These competing effects are prevalent in cluster environments.

How does the local environment affect the optical bar fraction, and where do barred galaxies live with respect to the density peaks in the supercluster environment? In this section, we make a first step in exploring these questions using four traces of local environment density: the line-of-sight projected surface mass density κ (Heymans et al. 2008), local galaxy number density Σ_{10} (WGM05, Gilmour et al. 2007), ICM density as characterized by the X-ray emission from hot intra-cluster gas, and the projected distance to the nearest cluster center. We calculate Σ_{10} by finding the radius enclosing the ten nearest neighbors to a galaxy. This is used to calculate a galaxy number density, quoted in $(Mpc/h)^{-2}$ (see Heiderman et al. 2008, in prep).

Figure 11 shows the variation of the three measures of local environment density (κ, Σ_{10}, and ICM density) with distance to the nearest cluster center. It is evident from all three tracers, that local density decreases with increasing distance from the nearest cluster center. We take the core radius to be at 0.25 Mpc, because the number density of galaxies shows a sharp break at this radius (Heiderman et al. 2008, in prep). The outer region is defined as lying between the core radius at R = 0.25 Mpc and the virial radius of the cluster, R_{vir} = 1.2 Mpc. Beyond the virial radius is the outskirt region.

Figure 12 shows the variation of the optical barred galaxy fraction function of: (a) distance from nearest cluster center, (b) log Σ_{10}, (c) κ, and (d) ICM density. We find *no strong trend of the optical bar fraction with local density for any of the tracers shown in Fig. 12. This result suggests that the optical bar fraction is not a strong function of the local environment.* Rather, the optical bar fraction and properties depend more strongly on the properties of the host galaxies (e.g., B/T, luminosity). This result is in agreement with recent results on bars in dense environments by Mendez-Abreu, Aguerri, & Corsini (2008), who find no variation of the optical bar fraction with Σ_{10}. The optical bar fraction shows a slight increase toward the innermost bin in panels b–d. In panel a, there is a slight increase in the optical bar fraction toward the cluster core, however number statistics are too low in the very innermost bin.

Several previous studies have found an enhanced optical bar fraction toward cluster centers (Barazza et al. 2008, in prep; Thomson 1981; Andersen 1996). Because bulge-dominated galaxies are prevalent in cluster cores and they have a lower optical bar fraction (§ 4.3), one might expect the optical bar fraction to be lower in the core region. However, galaxy interactions are more frequent, and these can induce bars, resulting in a higher bar fraction. Interestingly, higher bar fractions have been reported for groups of galaxies and binary pairs (e.g., Kumai et al. 1986; Elmegreen et al. 1990; Giuricin et al. 1993; Varela et al. 2004).

4.7. Comparison of the Optical Bar Fraction and Properties in the Supercluster and the Field

To understand what impact cluster processes have on the evolution of bars and disk galaxies, we must compare their properties to galaxies unaffected by such processes found in low density environments. We compare the results on bars and disks from the STAGES sample to those from the Ohio State University Bright Spiral Galaxy Survey (OSUBSGS; Eskridge et al. 2002) and the Sloan Digital Sky Survey (SDSS; Abazajian et al. 2004). Specifically, we use the results of MJ07, BJM08, and Aguerri (2008, in prep), where bars are identified and characterized through ellipse-fits. Before we compare the results obtained for bars in the cluster with those from the field studies, we must determine if the underlying galaxy populations in the samples are the same. Figure 13a–b shows the absolute M_V magnitude and rest-frame U-V color distributions of the STAGES, OSUBSGS, and SDSS samples. The OSUBSGS sample is brighter than both the SDSS and STAGES samples, and somewhat bluer than the STAGES sample. Also, it should be noted that the OSU survey is only complete for galaxies with M_V of -20.3 and brighter. The stellar mass distribution of the OSU, STAGES, and SDSS samples are over-plotted in Fig. 14. The masses for the OSU sample are calculated using the equation

$$M = V_{lum} \times 10^{(-0.628+1.305 \times BV - 0.10)}, \qquad (3)$$

where

$$V_{lum} = 10^{(-0.4 \times (M_V - 4.82)}, \qquad (4)$$

and BV is the B-V color (Bell et al. 2003). The OSU and STAGES samples have a similar range in stellar mass, however, the OSU sample is comprised of slightly more massive galaxies on average. The SDSS sample has a much narrower range in mass, with most galaxies lying between $M_*/M_\odot$ = $10^{9.5}$ and $10^{10.5}$, where the SDSS sample is complete. These are important caveats to keep in mind for the following analysis.

4.7.1. The Global Optical Bar Fraction

We have shown that the optical bar fraction is a strong function of B/T and luminosity, and somewhat a function of color. A comparison to the field is therefore non-trivial because of these factors. We attempt to compare to the same range of absolute magnitude and B/T galaxy type between the cluster and the field. We do not impose any color restrictions, because galaxies of the same luminosity and B/T can have a large color variation between cluster and the field.

The optical bar fraction in STAGES is found to be $\sim 30\% \pm 8\%$ for all methods of disk selection. The total optical bar fraction in OSUBSGS is 44% $\pm$ 7% (MJ07), and in the SDSS it is 48%–52% (BJM08). We cannot make a direct comparison of the OSU sample with the STAGES sample, because STAGES is dominated by much fainter galaxies and the OSU sample is only complete for galaxies brighter than $M_V \sim -20.3$ (Fig 13a). For the brighter subsample ($M_V \leq -20.3$), we find an optical bar fraction in STAGES of 47% $\pm$ 8% (58/124) and an optical bar

fraction in OSU of 40%± 8% (36/90). Thus, within the error margins, the optical bar fraction is comparable.

The SDSS sample is complete only for galaxies in the narrow magnitude range between $M_V = -18.6 - -20.5$, and the total optical bar fraction is 48%–52%. In the STAGES sample, the optical bar fraction for galaxies in the magnitude range $M_V = -18.6 - -20.5$, is 30%± 9% (65/211). **this comparison will be expanded ... note to Fabio - could you calculate a separate bar fraction in SDSS for bulge-dominated and disk dominated galaxies within the above magnitude range?**

Aguerri et al. (2008, in prep) study the bar fraction in the field from an SDSS sample at $0.01 < z < 0.4$, and find a total optical bar fraction of 45% for galaxies brighter than M_r of -20. This is comparable to our total optical bar fraction of 33%± 8% within the error margins. In addition, Aguerri et al. quoted an optical bar fraction of 30% for S0-type systems and 52% for late-type spirals (e.g., Sc-Sd). This is in agreement with our rough morphological visual classification, where we find that 25%± 8% of 'bulge+disk smooth' (e.g., S0) galaxies are barred, and 47%± 8% of 'pure disk' (e.g., Sc-Sd) galaxies are barred.

We have not found compelling evidence that the processes present in cluster environments directly affect the bar fraction. We have found that the cluster optical bar fraction is similar within ± 10% to the published field values for bright nearby galaxies (e.g., MJ07, BJM08, Aguerri et al. 2008, in prep). We have also found that the bar fraction does not show any strong trend with local density (see § 4.6). Our results suggest that the formation and/or destruction of a bar is strongly influenced by the properties of the host disk itself rather than on large-scale environmental effects.

4.7.2. *Bar Size and Strength Distribution*

Figure 15a–b shows the peak ellipticity e_{bar} distributions for the STAGES and OSUBSGS samples, respectively. In panel (a) the pink and green lines show the e_{bar} distributions for galaxies classified as 'bulge+disk' and 'pure disk', respectively. In panel (b) the distributions are split into bulge-dominated galaxies (S0-Sbc; pink) and (Sc-Sm; green). In both cases, galaxies with bulges appear to host weaker bars than galaxies with small bulges or no bulge at all. In addition, the bars in the STAGES supercluster sample have lower e_{bar} values overall than the bars from the OSUBSGS field sample. The result of lower e_{bar} in STAGES compared to OSU could be due to more bulge-dominated hosts in STAGES than OSU. Bars in galaxies with large bulges appear weaker (i.e., rounder). This effect has been observed in the STAGES sample, as well as in SDSS by BJMO8, and could be an artifact due to the dilution of the bar ellipticity by the bulge. It could also be an intrinsic effect.

We compare the e_{bar} distributions of the STAGES supercluster sample and the field SDSS sample in Figure 16a–b. For the STAGES galaxies, the e_{bar} distributions are split to show the blue-cloud and red-sequence, while the SDSS sample is comprised of blue-cloud galaxies only. It is evident in panel (a) that blue-cloud galaxies appear to host stronger bars than those on the red sequence. This result is likely caused by the same bulge-dilution ef-

fect discussed above, as 98% of the disk galaxies on the red-sequence are visually classified as 'bulge+disk'.

5. OPTICAL BAR FRACTION IN STARBURST AND NON-STARBURST GALAXIES

We may include one extra section to see if the optical bar fraction is higher in circumnuclear starburst versus non-starburst galaxies as expected theoretically, and as seen in the field. There are several issues here:
1) Starbursts (intense, short-lived episodes of SF) should really be defined as systems with high SFR and high SFR per unit *gas* mass (i.e, short gas consumption timescales), but we only have SFR per unit stellar mass (SSFR), which is not quite the same.
2) The theoretical prediction is for circumnuclear starbursts not global starbursts. One could get around this by citing results showing that most of the IR luminosity tends to come from the inner few kpc.
3) Issues on small fraction of sample with Spitzer detection.

6. SUMMARY AND CONCLUSIONS

We have used the STAGES $HST ACS$ survey of the Abell 901/902 supercluster in F606W at z~0.165 to study the properties of barred and unbarred disks in a dense environment. Ellipse-fitting was used to identify and characterize the properties of bars in our sample. Visual classification was used to characterize secondary morphological parameters such as the prominence of the bulge, clumpiness, and spiral arms. Galaxies were grouped into the broad classes: 'pure bulge', 'bulge+disk', and 'pure disk'. In addition, the galaxies were classified as either 'clumpy' or 'smooth'. To identify the optical bar fraction $f_{bar-opt}$, three methods of disk selection were used and compared: visual classification, color cut, and Sérsic cut. Using our sample of 475 moderately inclined ($i < 60°$), ellipse-fitted, bright ($M_V \leq$ -18), cluster galaxies, we find the following results.

1. *Disk selection in clusters:* In order to define the optical fraction of barred disk galaxies, we explore three methods of selecting moderately inclined ($i < 60°$) disk galaxies. We find 350, 256, and 199 such systems, respectively, via visual classification, a Sérsic cut ($n \leq 2.5$), and a blue-cloud cut. The traditional methods of disk selection such as taking a color cut or Sérsic cut, are problematic in a cluster environment. A color cut misses 50%± 4% of visually-identified disk galaxies. A Sérsic cut misses 36%± 4% of disk galaxies with $n > 2.5$. Therefore, a blind application of a color cut or Sérsic cut would miss many red, bulge-dominated galaxies that are prevalent in a cluster environment.

2. *Global optical bar fraction:* For the three methods of disk selection (visual, color cut, Sérsic cut), we obtain a similar optical bar fraction $f_{bar-opt}$ of 33%± 8%, 29%± 8%, and 28%± 8%, respectively. We explore $f_{bar-opt}$ as a function of host galaxy properties and find that it rises in brighter galaxies and/or those which are less bulge-dominated. Within a given M_V bin, $f_{bar-opt}$ is higher in

visually-selected disk galaxies that have no bulge as opposed to those with bulges. Conversely, for a given visual morphological class, $f_{bar-opt}$ rises at higher luminosities. Both results are similar to trends found in the field. We find no significant trend of $f_{bar-opt}$ with local environment density tracers such as κ, Σ_{10}, ICM density, and projected distance to the nearest cluster center. Furthermore, the cluster optical bar fraction is similar within $\pm$ 10% to the published field values for bright nearby galaxies, for SDSS early Hubble type systems, and faint disk dominated galaxies. Our results suggest that the optical bar fraction is not a strong function of local environment.

3. *Optical bar fraction as a function of B/T and luminosity:*

We explore $f_{bar-opt}$ as a function of host galaxy properties and find that it rises in spiral galaxies, which are less bulge-dominated and/or are brighter. The optical bar fraction is a factor of $\sim$ 1.8 higher in galaxies classified as 'pure disk' compared to galaxies visually classified as 'bulge+disk'. When the normalized effective radius r_e/a_{disk} is used to trace central galaxy concentration, the bar fraction is $\sim$ 2.7 times higher in galaxies with the lowest central concentration ($r_e/a_{disk} = 0.75$) compared to the galaxies with the highest central concentration ($r_e/a_{disk} = 0.15$). In fact, *within a given M_V bin, $f_{bar-opt}$ is higher in visually-selected disk galaxies that have no bulge as opposed to those with bulges.* Furthermore, we find that for a given visual morphological class, $f_{bar-opt}$ rises at higher luminosities.

4. *Optical bar fraction as a function of κ, Σ_{10}, ICM density, and distance from nearest cluster center:* We find no strong trend of the fraction of barred disks with any of the four traces of environment density. However, there is a weak increase in the

optical bar fraction inside the core radius of the clusters. This may be tied to the triggering of bars by frequent tidal interactions in the dense cluster cores.

5. *Comparison to field studies:* We compare our results to those for field samples, specifically MJ07 (OSUBSGS), BJM08 (SDSS), and Aguerri et al. (SDSS; 2008, in prep), where bar identification and characterization was done in the same way as for the STAGES sample. If we consider only galaxies with $M_V > -20.3$ in both the STAGES and OSUBSGS samples, then we obtain a bar fraction in STAGES of 47%$\pm$ 8% and a bar fraction in OSU of 40%$\pm$ 8%. Thus for the brightest galaxies, the bar fraction is comparable within the range of uncertainty. Our results also agree with those of Aguerri et al. (SDSS; 2008, in prep) for early-type bulge-dominated galaxies and very late-type disk dominated galaxies.

REFERENCES

Abazajian, K., et al. 2004, AJ, 128, 502
Abraham, R. G., et al. 1996, ApJ, 471, 694
Andersen, V. 1996, AJ, 111, 1805
Athanassoula, E. 1992, MNRAS, 259, 345
Athanassoula, E. 2002, ApJL, 569, L83
Athanassoula, E. 2005, MNRAS, 358, 1477
Athanassoula, E., Lambert, J. C., & Dehnen, W. 2005, MNRAS, 363, 496
Aguerri, J. A. L., Mendez-Abreu, J., & Corsini, E. M., 2008, A&A, in preparation
Balogh, M. L., Schade, D., Morris, S. L., Yee, H. K. C., Carlberg, R. G., & Ellingson, E. 1998, ApJL, 504, L75
Balogh, M. L., Morris, S. L., Yee, H. K. C., Carlberg, R. G., & Ellingson, E. 1999, ApJ, 527, 54
Balogh, M. L., Navarro, J. F., & Morris, S. L. 2000, ApJ, 540, 113
Barden, M., et al. 2005, ApJ, 635, 959
Bekki, K. 1999, ApJL, 510, L15
Bell, E. F., McIntosh, D. H., Katz, N., & Weinberg, M. D. 2003, ApJS, 149, 289
Bell, E. F., et al. 2004, ApJL, 600, L11
Bell, E. F., et al. 2005, ApJ, 625, 23
Binggeli, B., Sandage, A., & Tammann, G. A. 1988, ARAA, 26, 509
Binney, J., & Tremaine, S. 1987, Princeton, NJ, Princeton University Press, 1987, 747 p.,
Blanton, M. R., Eisenstein, D., Hogg, D. W., Schlegel, D. J., & Brinkmann, J. 2005, ApJ, 629, 143
Borch, A., et al. 2006, A&A, 453, 869

Bravo-Alfaro, H., Cayatte, V., van Gorkom, J. H., & Balkowski, C. 2000, AJ, 119, 580
Bureau, M., & Freeman, K. C. 1999, AJ, 118, 126
Bureau, M., & Athanassoula, E. 2005, ApJ, 626, 159
Buta, R., Vasylyev, S., Salo, H., & Laurikainen, E. 2005, AJ, 130, 506
Butcher, H., & Oemler, A., Jr. 1978, ApJ, 219, 18
Byrd, G., & Valtonen, M. 1990, ApJ, 350, 89
Cayatte, V., van Gorkom, J. H., Balkowski, C., & Kotanyi, C. 1990, AJ, 100, 604
Combes, F., Debbasch, F., Friedli, D., & Pfenniger, D. 1990, A&A, 233, 82
Combes, F., & Sanders, R. H. 1981, A&A, 96, 164
Das, M., & Jog, C. J. 1995, ApJ, 451, 167
Debattista, V. P., & Sellwood, J. A. 1998, ApJL, 493, L5
Debattista, V. P., & Sellwood, J. A. 2000, ApJ, 543, 704
Debattista, V. P., Mayer, L., Carollo, C. M., Moore, B., Wadsley, J., & Quinn, T. 2006, ApJ, 645, 209
de Vaucouleurs, G. 1963, ApJS, 8, 31
de Vaucouleurs, G., de Vaucouleurs, A., Corwin Jr., H. G., Buta, R. J., Paturel, G., & Fouque, P. 1991, Third Reference Catalogue of Bright Galaxies (New York: Springer) (RC3)
Dubinski, J., Gauthier, J.-R., Widrow, L., & Nickerson, S. 2008, ArXiv e-prints, 802, arXiv:0802.3997
Dressler, A. 1980, ApJ, 236, 351
Elmegreen, B. G. 1979, ApJ, 231, 372

Elmegreen, D. M., Elmegreen, B. G., & Bellin, A. D. 1990, ApJ, 364, 415

Elmegreen, B. G. 1994, ApJL, 425, L73

Elmegreen, B. G., Elmegreen, D. M., & Hirst, A. C. 2004, ApJ, 612, 191

Eskridge, P. B., et al. 2000, AJ, 119, 536

Evrard, A. E., Silk, J., & Szalay, A. S. 1990, ApJ, 365, 13

Fisher, D. B. 2006, ApJL, 642, L17

Friedli, D., Wozniak, H., Rieke, M., Martinet, L., & Bratschi, P. 1996, A&A Suppl., 118, 461

Giuricin, G., Mardirossian, F., Mezzetti, M., & Monaco, P. 1993, ApJ, 407, 22

Graham, A. W., & Worley, C. C. 2008, MNRAS, 752

Gray, M. E., Taylor, A. N., Meisenheimer, K., Dye, S., Wolf, C., & Thommes, E. 2002, ApJ, 568, 141

Gunn, J. E., & Gott, J. R. I. 1972, ApJ, 176, 1

Hernquist, L., & Mihos, J. C. 1995, ApJ, 448, 41

Heymans, C., et al. 2008, MNRAS, 385, 1431

Hunt, L. K., & Malkan, M. A. 1999, ApJ, 516, 660

Jedrzejewski, R. I. 1987, MNRAS, 226, 747

Jogee, S. 1999, Ph.D. thesis, Yale University

Jogee, S., Knapen, J. H., Laine, S., Shlosman, I., Scoville, N. Z., & Englmaier, P. 2002a, ApJL, 570, L55

Jogee, S., Shlosman, I., Laine, S., Knapen, J. H., Englmaier, P., Scoville, N. Z., & Wilson, C. D. 2002b, ApJ

Jogee, S., Barazza, F., Rix, H.-W., Shlosman, I. et al. 2004a, ApJl, 615, L105

Jogee, S., Scoville, N., & Kenney, J. D. P. 2005, ApJ, 630, 837

Kennicutt, R. C., Jr. 1998, ARAA, 36, 189

Knapen, J. H., Shlosman, I., & Peletier, R. F. 2000, ApJ, 529, 93

Kodama, T., & Smail, I. 2001, MNRAS, 326, 637

Koopmann, R. A., & Kenney, J. D. P. 1998, ApJL, 497, L75

Koopmann, R. A., Kenney, J. D. P., & Young, J. 2001, ApJS, 135, 125

Kormendy, J. 1982, ApJ, 257, 75

Kormendy, J. 1993, Galactic Bulges, 153, 209

Kormendy, J., & Kennicutt, R. C., Jr. 2004, ARAA, 42, 603

Kuijken, K., & Merrifield, M. R. 1995, ApJL, 443, L13

Kumai, Y., Taniguchi, Y., & Ishii, H. 1986, MNRAS, 223, 139

Lacey, C., & Silk, J. 1991, ApJ, 381, 14

Laine, S., Kenney, J. D. P., Yun, M. S., & Gottesman, S. T. 1999, ApJ, 511, 709

Laine, S., Shlosman, I., Knapen, J. H., & Peletier, R. F. 2002, ApJ, 567, 97

Larson, R. B., Tinsley, B. M., & Caldwell, C. N. 1980, ApJ, 237, 692

Laurikainen, E., Salo, H., & Buta, R. 2004, ApJ, 607, 103

Laurikainen, E., Salo, H., Buta, R., & Vasylyev, S. 2004, MNRAS, 355, 1251

Laurikainen, E., Salo, H., Buta, R., & Knapen, J. H. 2007, MNRAS, 381, 401

Lütticke, R., Dettmar, R.-J., & Pohlen, M. 2000, A&A Suppl., 145, 405

Margoniner, V. E., de Carvalho, R. R., Gal, R. R., & Djorgovski, S. G. 2001, ApJL, 548, L143

Marinova, I., & Jogee, S. 2007, ApJ, 659, 1176

Martinez-Valpuesta, I., Shlosman, I., & Heller, C. 2006, ApJ, 637, 214

McIntosh, D. H., et al. 2005, ApJ, 632, 191

Méndez-Abreu, J., Aguerri, J. A. L., & Corsini, E. M. 2008, ArXiv e-prints, 802, arXiv:0802.0011

Menéndez-Delmestre, K., Sheth, K., Schinnerer, E., Jarrett, T. H., & Scoville, N. Z. 2007, ApJ, 657, 790

Mihos, J. C., Walker, I. R., Hernquist, L., Mendes de Oliveira, C., & Bolte, M. 1995, ApJL, 447, L87

Moore, B., Katz, N., Lake, G., Dressler, A., & Oemler, A. 1996, Nature, 379, 613

Moore, B., Lake, G., & Katz, N. 1998, ApJ, 495, 139

Mulchaey, J. S., & Regan, M. W. 1997, ApJL, 482, L135

Norman, C. A., Sellwood, J. A., & Hasan, H. 1996, ApJ, 462, 114

Odewahn, S. C. 1996, ASP Conf. Ser. 91: IAU Colloq. 157: Barred Galaxies, 91, 30

Oemler, A. J. 1974, ApJ, 194, 1

Quillen, A. C., Frogel, J. A., Kenney, J. D. P., Pogge, R. W., & Depoy, D. L. 1995, ApJ, 441, 549

Quinn, P. J., Hernquist, L., & Fullagar, D. P. 1993, ApJ, 403, 74

Ravindranath, S., et al. 2004, ApJL, 604, L9

Reese, A. S., Williams, T. B., Sellwood, J. A., Barnes, E. I., & Powell, B. A. 2007, AJ, 133, 2846

Regan, M. W., Vogel, S. N., & Teuben, P. J. 1997, ApJ, 482, L143

Sakamoto, K., Okumura, S. K., Ishizuki, S., & Scoville, N. Z. 1999, ApJ, 525, 691

Schwarz, M. P. 1981, ApJ, 247, 77

Sellwood, J. A. 1993, Galactic Bulges, 153, 391

Sellwood, J. A., & Wilkinson, A. 1993, Reports of Progress in Physics, 56, 173

Sérsic, J. L., & Pastoriza, M. 1967, PASP, 79, 152

Shen, J., & Sellwood, J. A. 2004, ApJ, 604, 614

Sheth, K., Regan, M. W., Scoville, N. Z., & Strubbe, L. E. 2003, ApJL, 592, L13

Sheth, K., Vogel, S. N., Regan, M. W., Thornley, M. D., & Teuben, P. J. 2005, ApJ, 632, 217

Sheth, K., et al. 2008, ApJ, 675, 1141

Shlosman, I., Frank, J., & Begelman, M. C. 1989, Nature, 338, 45

Shlosman, I., & Noguchi, M. 1993, ApJ, 414, 474

Thompson, L. A. 1981, ApJL, 244, L43

Toomre, A. 1981, Structure and Evolution of Normal Galaxies, 111

Treu, T., Ellis, R. S., Kneib, J.-P., Dressler, A., Smail, I., Czoske, O., Oemler, A., & Natarajan, P. 2003, ApJ, 591, 53

van den Bergh, S. 2002, AJ, 124, 782

van den Bergh, S. 2007, AJ, 134, 1508

van Kampen, E., & Katgert, P. 1997, MNRAS, 289, 327

Varela, J., Moles, M., Márquez, I., Galletta, G., Masegosa, J., & Bettoni, D. 2004, A&A, 420, 873

Vollmer, B., Braine, J., Combes, F., & Sofue, Y. 2005, A&A, 441, 473

Weinberg, M. D. 1985, MNRAS, 213, 451

Weinzirl, T., Jogee, S., Khochfar, S., Burkert, A., & Kormendy, J. 2008, ArXiv e-prints, 807, arXiv:0807.0040

Wolf, C., et al. 2004, A&A, 421, 913

Wolf, C., Gray, M. E., & Meisenheimer, K. 2005, A&A, 443, 435

Wozniak, H., Friedli, D., Martinet, L., Martin, P., & Bratschi, P. 1995, A&A Suppl., 111, 115

Zabludoff, A. I., & Franx, M. 1993, AJ, 106, 1314

Zheng, X. Z., Hammer, F., Flores, H., Assémat, F., & Rawat, A. 2005, A&A, 435, 507

TABLE 1

OPTICAL BAR FRACTION FROM DIFFERENT METHODS TO IDENTIFY DISK GALAXIES AMONG $M_V \leq -18$, $i < 60°$ SYSTEMS

Method	N_{disk}	N_{barred}	$f_{bar,opt}$
Visual	350	115	33% ± 8%
Color	199	58	29% ± 8%
Sérsic	256	72	28% ± 8%

Note. — All optical bar fractions are for galaxies with $M_V \leq -18$. Columns are: (1) Method for selecting disk galaxies. See § 3.2 and § 4.1 for details; (2) Number of disk galaxies, N_{disk}; (3) Number of barred disk galaxies, N_{barred}. Bars are detected through ellipse fitting; (4) Optical bar fraction, $f_{bar-opt}$, defined as in Eq. 1. Error bars include the sum in quadrature of the binomial term in the statistical error and the uncertainty caused by isophotal twists, causing bars to be missed by ellipse-fitting.

TABLE 2

OPTICAL BAR FRACTION FROM DIFFERENT METHODS TO IDENTIFY DISK GALAXIES AMONG $M_*/M_\odot \geq 10^9$, $i < 60°$ SYSTEMS

Method	N_{disk}	N_{bar}	$f_{bar,opt}$
Visual	409	130	33% ± 8%
Color	226	70	31% ± 8%
Sérsic	321	88	27% ± 8%

Note. — All optical bar fractions are for galaxies with $M_*/M_\odot > 10^9$. Columns are: (1) Method for selecting disk galaxies. See § 3.2 and § 4.1 for details; (2) Number of disk galaxies, N_{disk}; (3) Number of barred disk galaxies, N_{barred}. Bars are detected through ellipse fitting; (4) Optical bar fraction, $f_{bar-opt}$, defined as in Eq. 1. Error bars include the sum in quadrature of the binomial term in the statistical error and the uncertainty caused by isophotal twists, causing bars to be missed by ellipse-fitting.

TABLE 3

OPTICAL BAR FRACTION AS A FUNCTION OF VISUALLY CLASSIFIED SECONDARY MORPHOLOGICAL PARAMETERS

	N_{all}	N_{disk}	N_{bar}	$f_{bar,opt}$
Pure bulge	116	—	—	—
B+D	$111^a + 135^b + 23^c$	269	77	29% ± 8%
Pure disk	81	81	38	47% ± 8%
Clumpy	105	105	47	45% ± 8%
Smooth	361	245	68	28% ± 8%

Note. — Columns are : (1) Morphological parameters from visual classification (a - number of 'bulge+disk' galaxies with bar/spiral arm; b - number of 'bulge+disk' galaxies without bar/spiral; c - number of bulge+disk galaxies without bar and no spiral arm class); (2) Total number of galaxies in class; (3) Number of *disk* galaxies in class; (4) Number of barred disk galaxies, where bars are from ellipse fitting; (5) Optical bar fraction calculated as in Eq. 1.
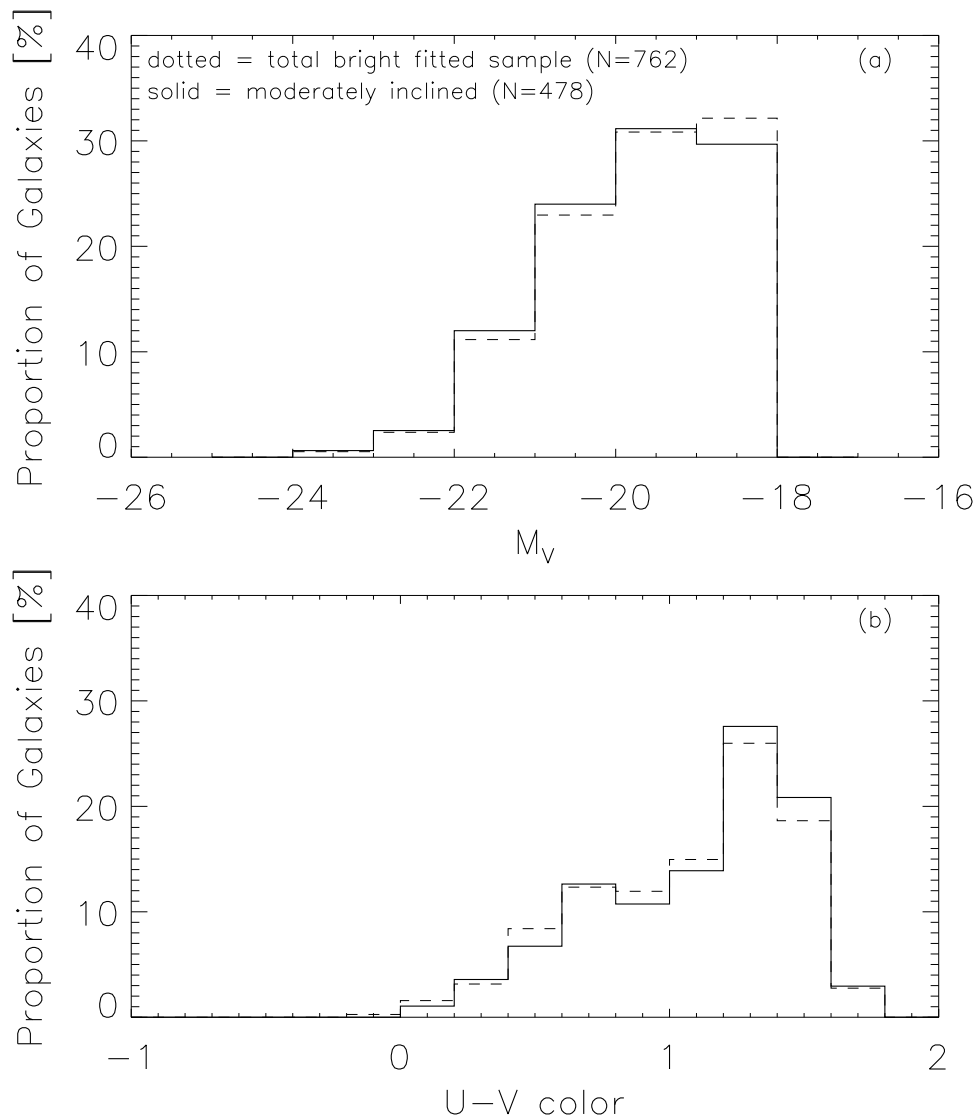
FIG. 1.— (a) The dotted line shows the histogram of M_V absolute magnitude of our cluster sample of 762 ellipse-fitted, bright ($M_V \leq -18$) galaxies. Most galaxies have $-20 \leq M_V \leq -18$. The solid line shows the M_V distribution of the final cluster sample, after excluding highly inclined ($i > 60°$), and poorly fitted galaxies. (b) Rest-frame $U - V$ color distribution of the whole ellipse-fitted sample of 762 galaxies (dotted line) and final sample, after excluding highly inclined galaxies and bad fits (475 galaxies; solid line). Excluding the highly inclined galaxies does not have a significant effect on the absolute M_V magnitude, or rest-frame $U - V$ color distributions.
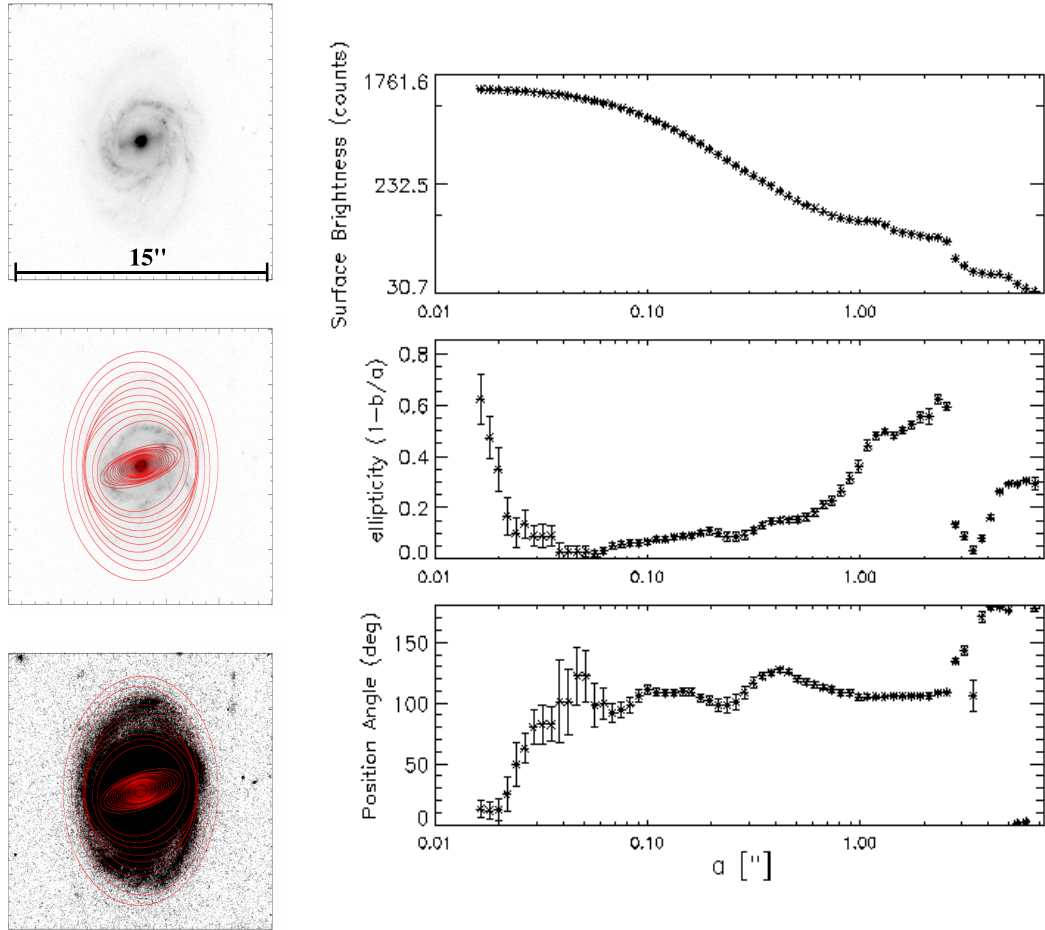
Fig. 2.— *Left*: Ellipse fit overlays on the F606W image of a barred cluster galaxy. In the middle and bottom panels, the contrast is adjusted to show the inner regions and outer disk regions, respectively. *Right*: Radial profiles of the surface brightness (SB), ellipticity *e*, and position angle (PA). The bar signature is evident in the smooth rise of the *e* to a global maximum, while the PA remains relatively constant in the bar region. The *e* then drops and the PA changes, indicating the transition to the disk region. See § 3.1 for details.
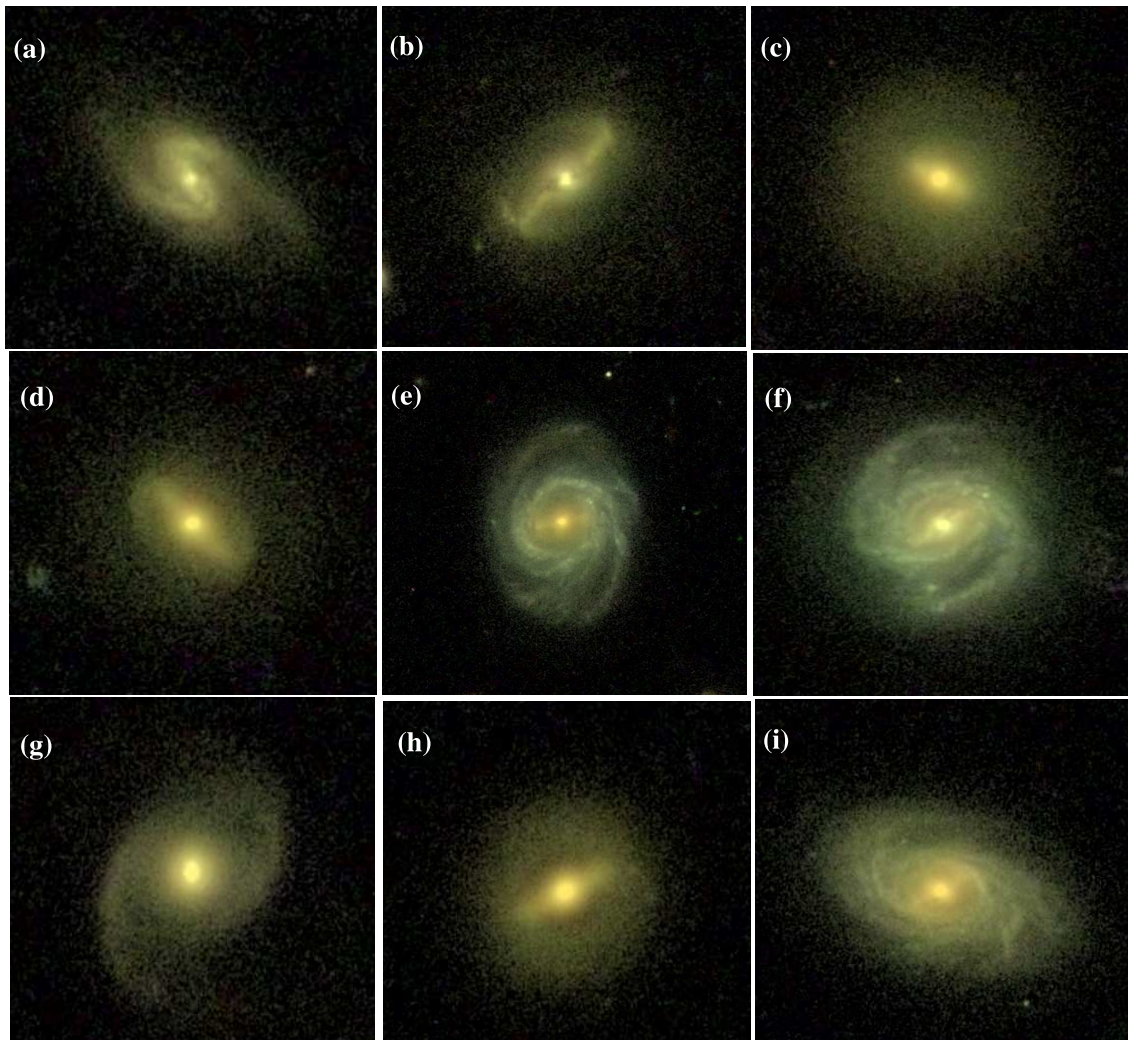
FIG. 3.— Examples of representative bright ($M_{\rm V} \leq -18$) barred galaxies identified through ellipse-fitting in the A901/902 supercluster.

16
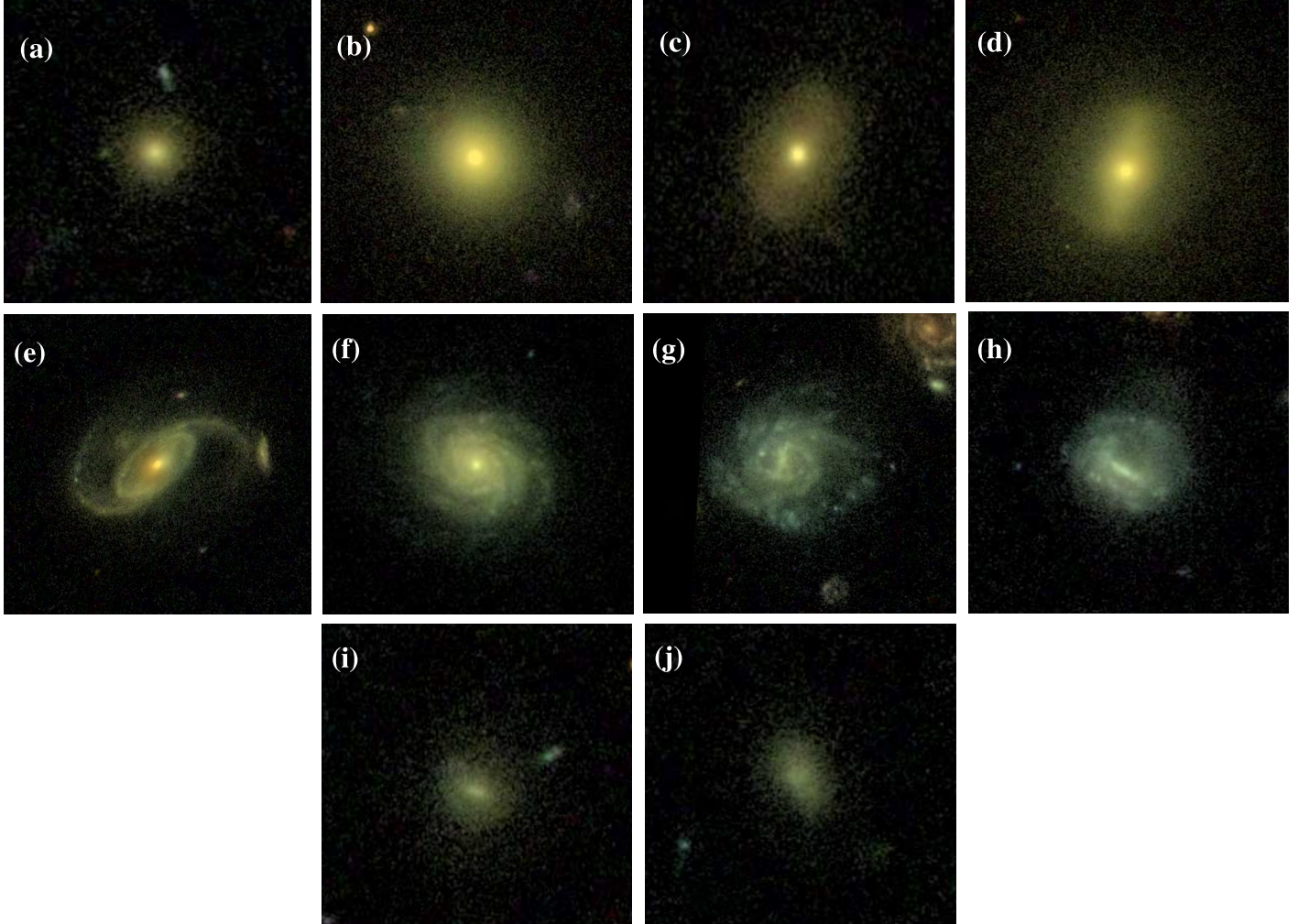
FIG. 4.— Examples of the visual classification of secondary morphological properties (§ 3.3) for the bright ($M_{\rm V} \leq -18$), moderately inclined ($i < 60°$) sample. Galaxies are grouped according to the visual prominence of the bulge into three groups: 'pure bulge' (a,b), 'bulge+disk' (c–f), and 'pure disk' (g–j). Note that it is difficult to visually separate the classes 'pure bulge' and 'bulge+disk' (e.g., b vs. c) when the galaxy appears smooth and shows no disk signatures such as bars or spiral arms.
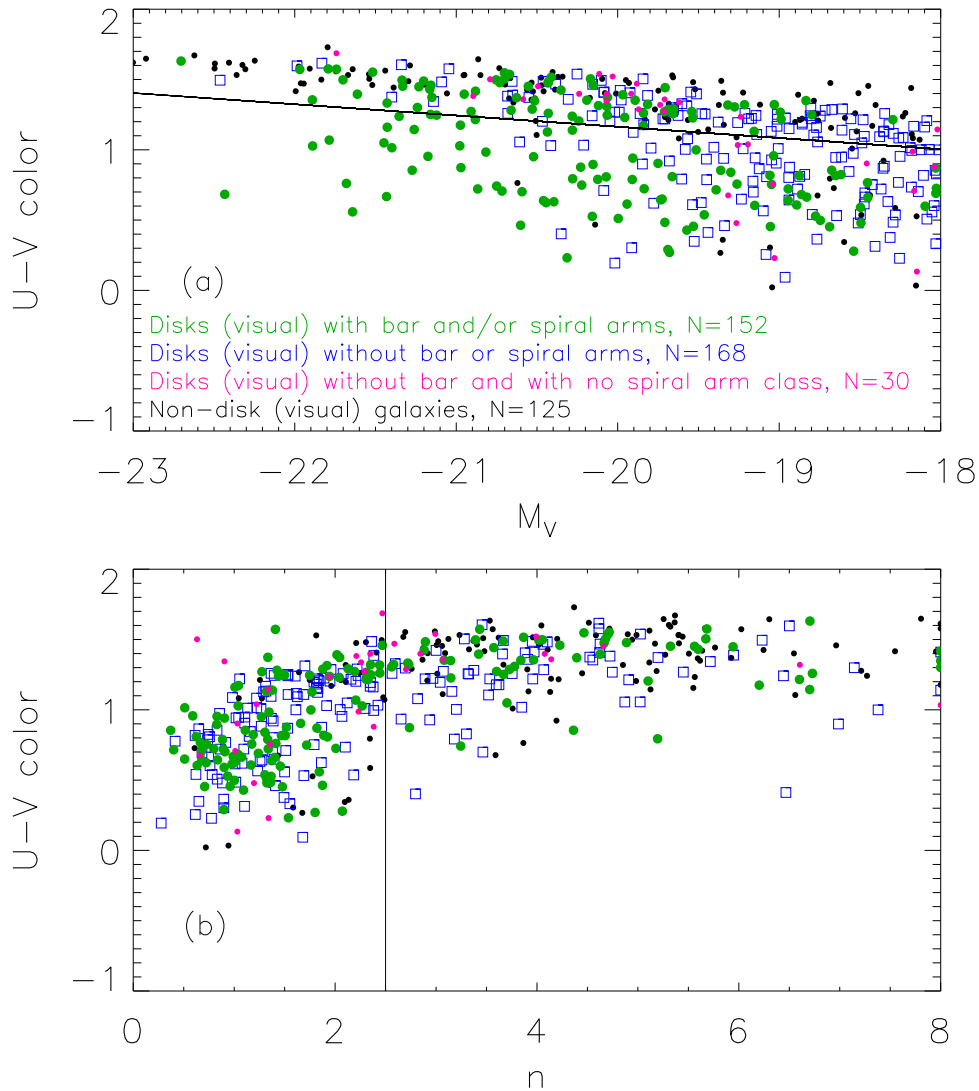
Fɪɢ. 5.— This figure compares the disk galaxies identified through three different methods: visual classification, blue-cloud color cut, and a Sérsic cut for the bright ($M_V \leq -18$), moderately inclined ($i < 60°$) sample. Panel (a) shows where the visually identified disk galaxies (filled circles and open squares) lie in the rest-frame $U - V$ vs. M_V plane. The systems are further split into disk galaxies with a bar and/or spiral arms (filled circles) and ones without (open squares). The pink points show visually-identified, unbarred disk galaxies that had no spiral arm classification. The black points represent all other galaxies, not classified as disks. The solid line separates the red sequence from the blue cloud galaxies. A blue-cloud color cut selecting disks only below this line captures 178 out of 350 visually-identified disk galaxies. The remaining 172 or ∼ 50%± 4% of visually-identified disks lie on the red sequence. Panel (b) shows where visually identified disk galaxies lie in the Sérsic index n vs. M_V plane. Colors are the same as in panel (a). The solid line shows the cutoff of $n = 2.5$, which is supposed to separate disk galaxies and spheroids. Again, if such a cut is used to select disks, 223 of the visually-identified disks are captured, but the remaining 127 (36%± 4%) with n> 2.5 are missed.
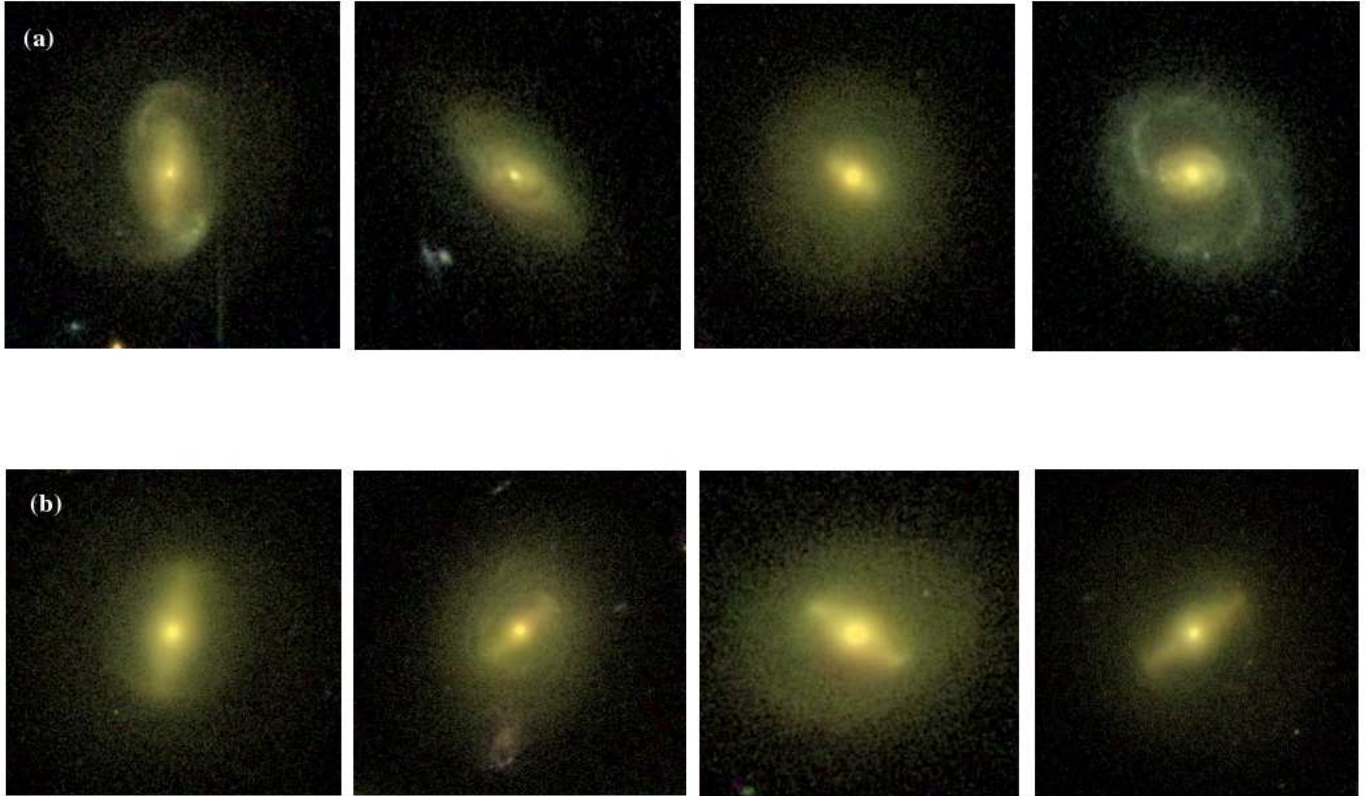
FIG. 6.— Examples of bright ($M_{\rm V} \leq -18$), moderately inclined ($i < 60°$), visually-identified disk galaxies missed by a Sérsic cut with $n \leq 2.5$ (a) and blue-cloud cut (b).
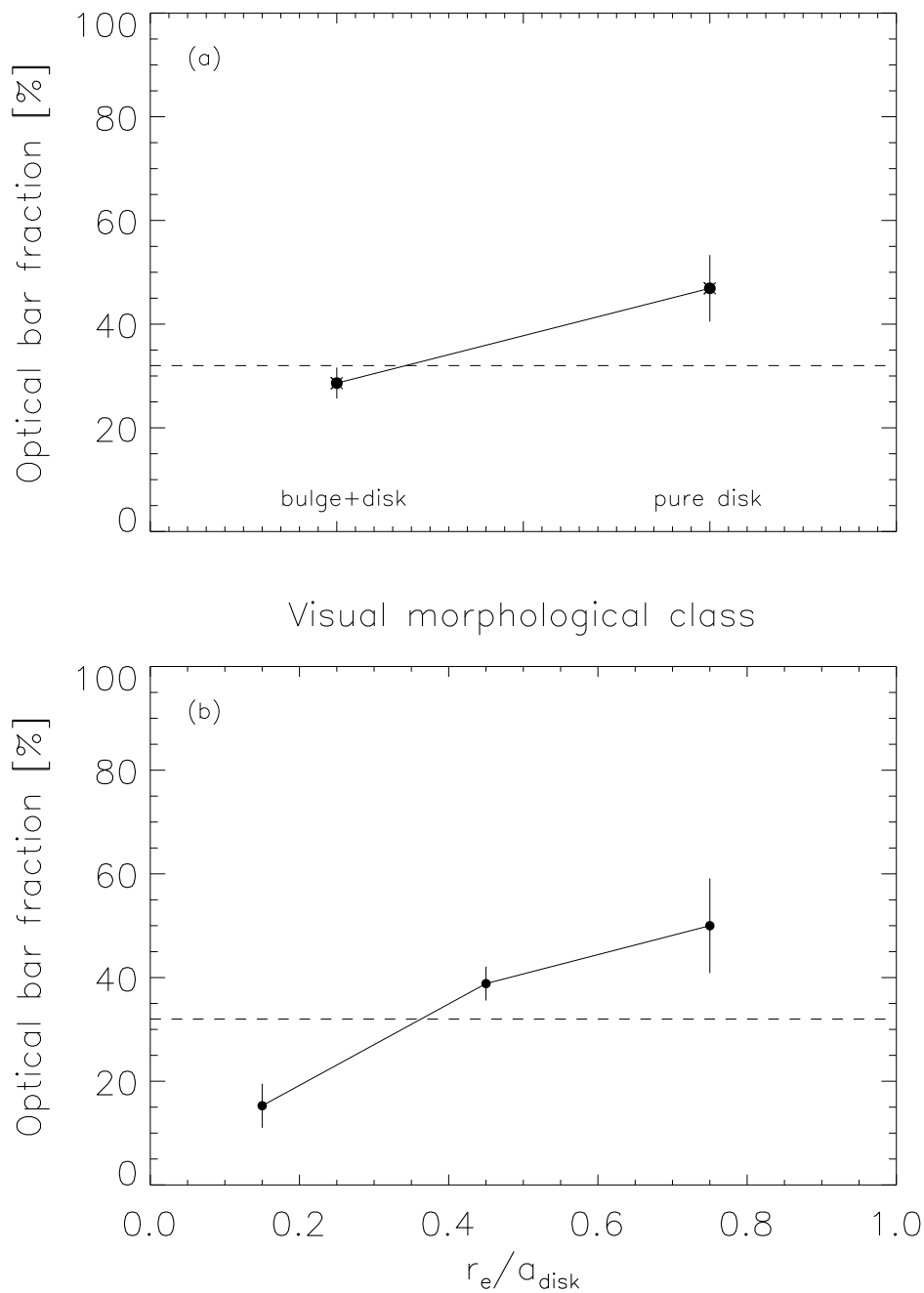
FIG. 7.— (a) The optical bar fraction as a function of visual morphological class. The total bar fraction (32%± 8%) using visual disk selection is shown as the horizontal dashed line in both panels. The first bin contains galaxies classified as 'bulge+disk', while the second bin contains galaxies classified as 'pure disk'. The bar fraction shows a rise from 29%± 3% to 47%± 6% from galaxies classified as 'bulge+disk' to 'pure disk'. The error bars represent the statistical errors in each bin. (b) The optical bar fraction as a function of central galaxy concentration, as characterized by the effective radius normalized to the disk radius, r_e/a_{disk}. Only bins with significant number statistics are shown. The bar fraction increases from 15%± 8% in galaxies with high concentration ($r_e/a_{disk} \sim 0.15$), to 50%± 12% in galaxies with low concentration ($r_e/a_{disk} \sim 0.75$). Again, the error bars show the statistical Poisson errors in each bin.
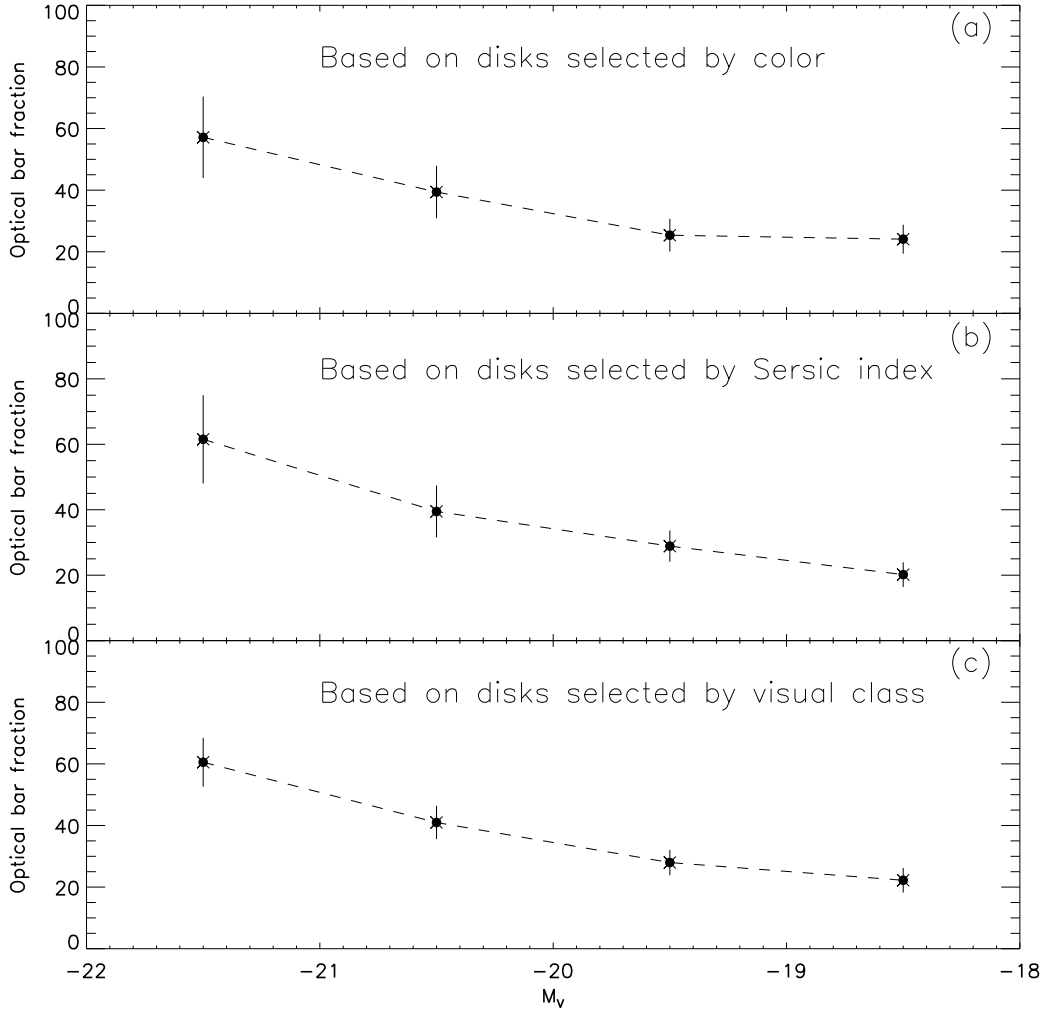
FIG. 8.— We plot the optical bar fraction as a function of galaxy luminosity M_V for the three methods of disk selection: (a) a blue-cloud color cut; (b) a Sérsic (n≤ 2.5) cut; (c) visual classification. For all three methods of disk selection, the optical bar fraction shows a decrease from $\sim 60\%\pm 10\%$ at $M_V \sim -21.5$ to $\sim 20\%\pm 5\%$ at $M_V = -18.5$. The error bars show the statistical Poisson errors in each bin.
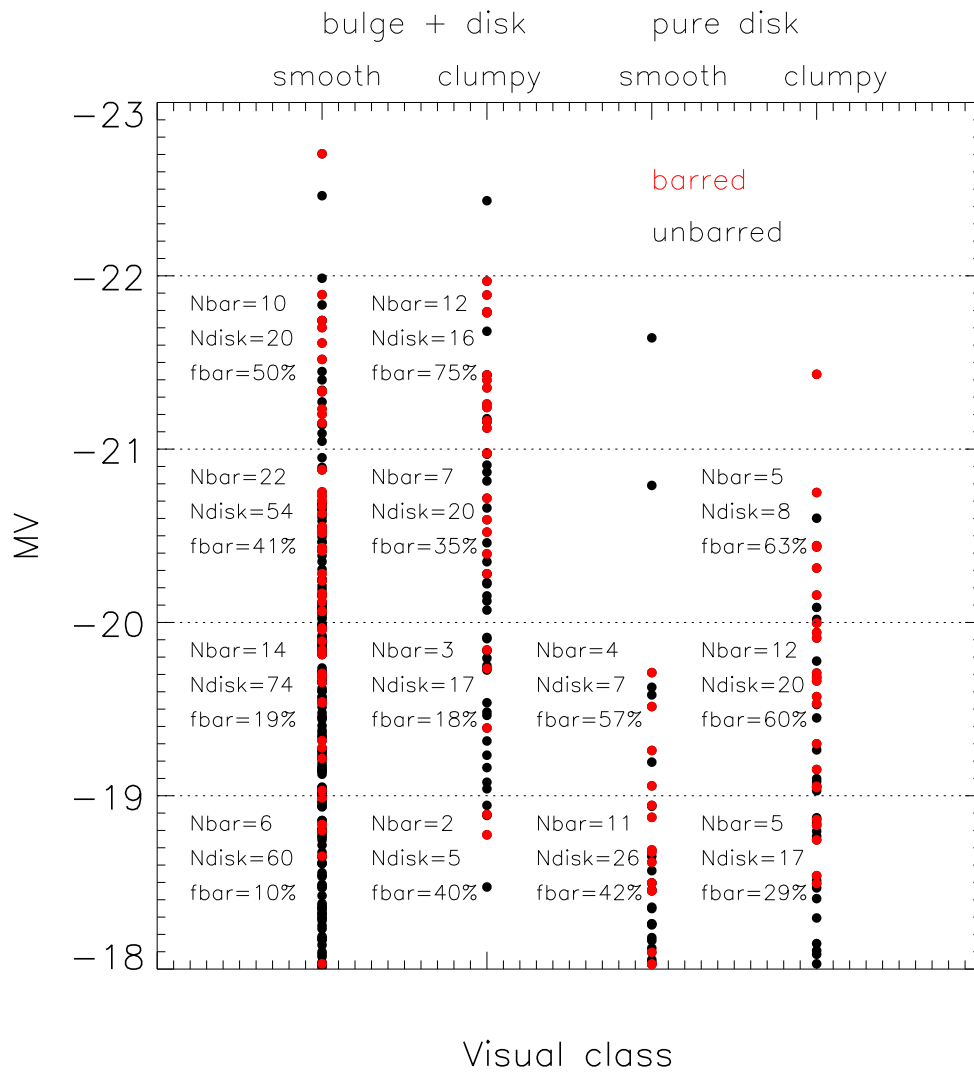
21

Fig. 9.— We show the optical bar fraction in a two-dimensional parameter space defined by morphological class and luminosity. Here, the morphological classes refer to the four visually-classified disk morphological classes: bulge+disk smooth, bulge+disk clumpy, pure disk smooth, and pure disk clumpy. It is evident that *within a given morphological class*, the bar fraction increases at brighter M_V. Also, at a given absolute magnitude, the bar fraction increases for disk-dominated galaxies. Thus, the optical bar fraction depends on both luminosity and the relative bulge-to-disk ratio of a disk galaxy.

22
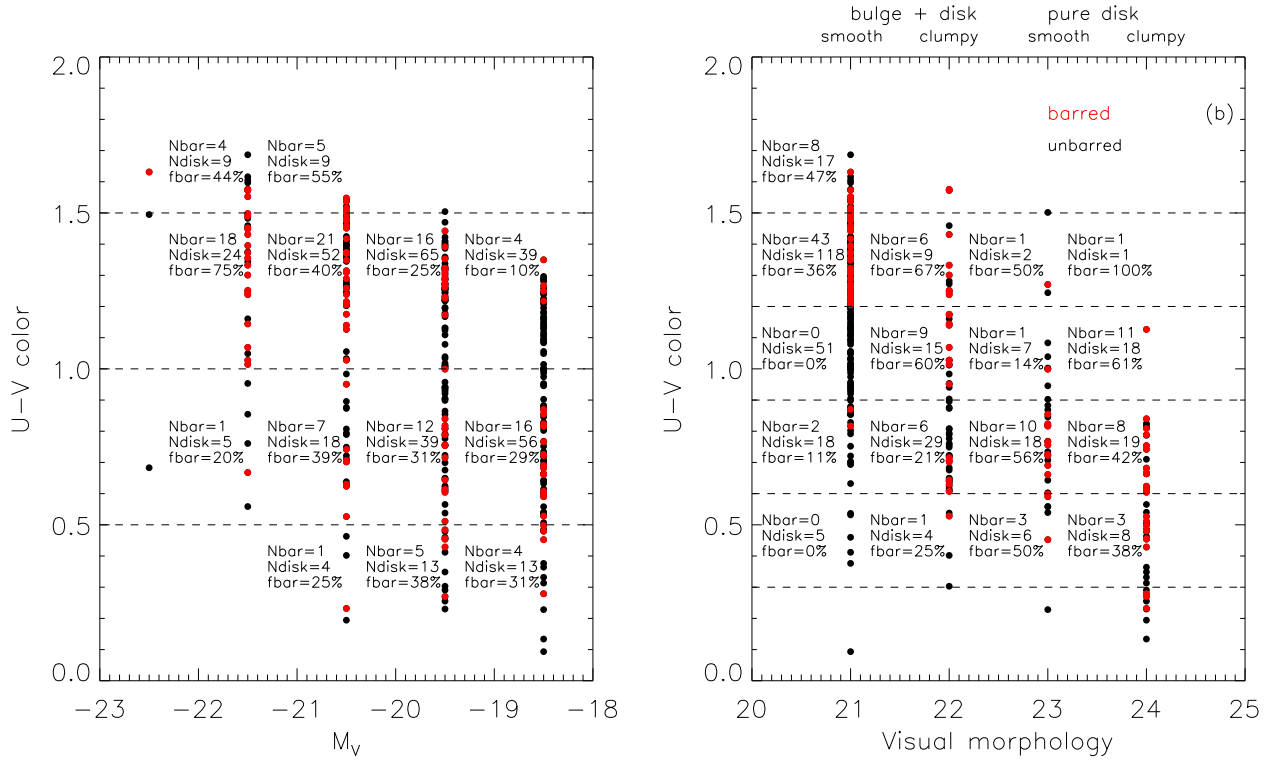
FIG. 10.— The optical bar fraction is shown in the rest-frame $U-V$ color vs M_V plane (**left**), and the rest-frame $U-V$ color vs disk morphological class (**right**). Here the morphological classes refer to the four visually-classified disk morphological classes: bulge+disk smooth, bulge+disk clumpy, pure disk smooth, and pure disk clumpy.
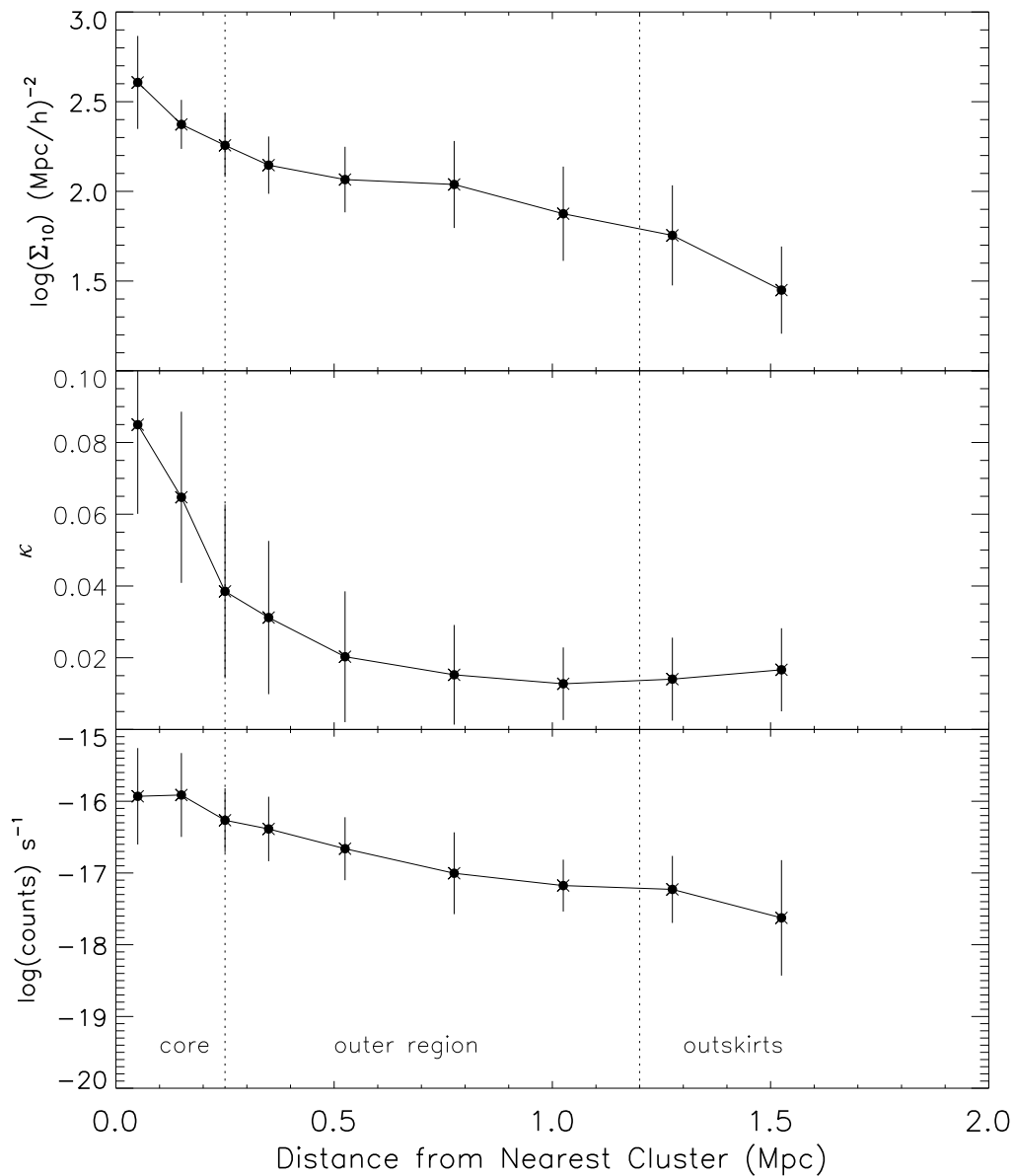
FIG. 11.— We plot the variation of the three measures of environment density (κ, Σ_{10}, ICM density) as a function of distance to the nearest cluster center. All three measures show a decrease in density as a function of cluster-centric distance. The vertical dashed lines denote the core radius at 0.25 Mpc and the virial radius at 1.2 Mpc. The error bars show the statistical Poisson errors in each bin.

24
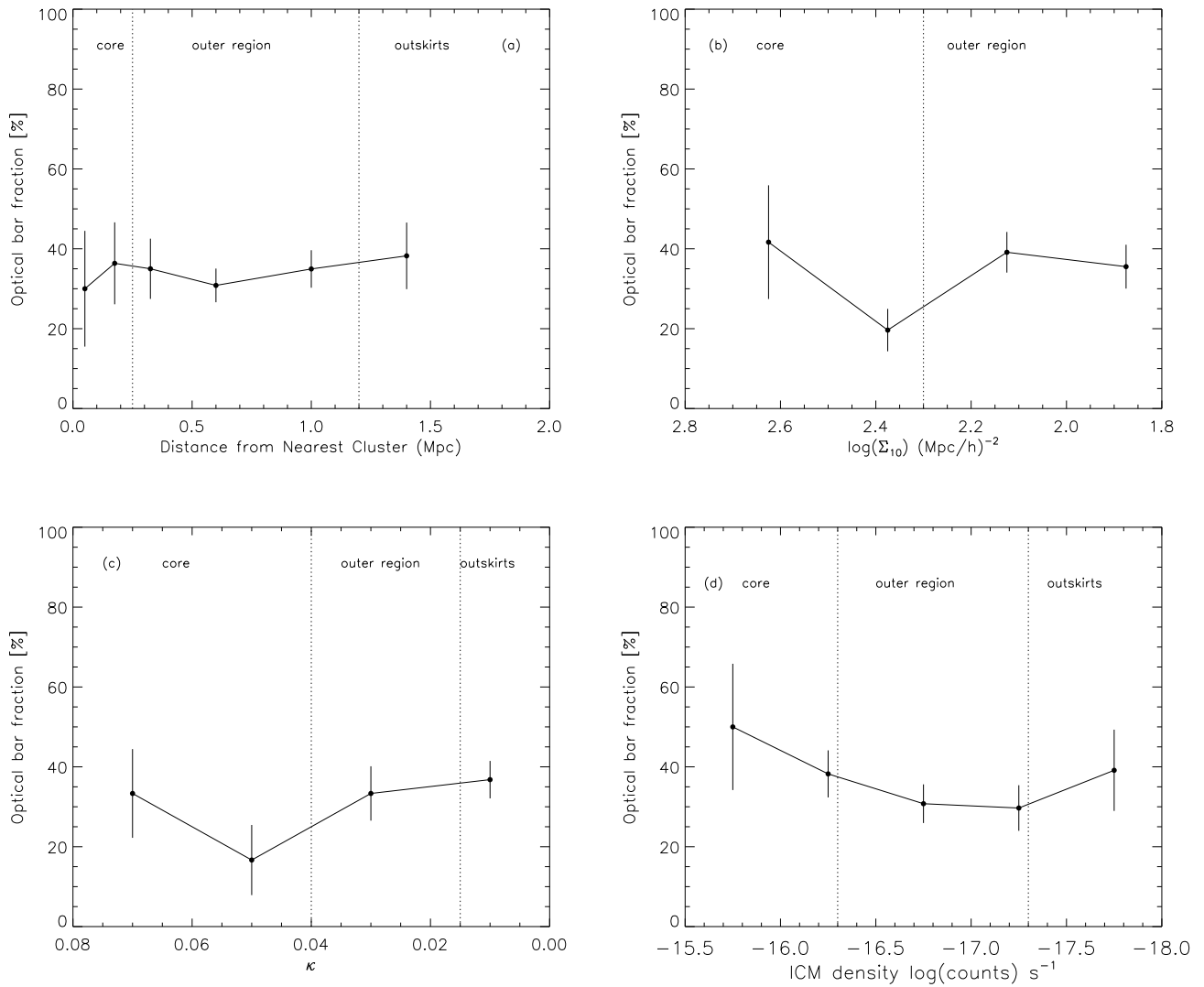
FIG. 12.— The fraction of barred galaxies a function of: (a) distance from nearest cluster center, (b) logΣ_{10}, (c) κ, and (d) ICM density. Bar classifications are from ellipse fits and disks are identified by visual classification. The vertical dashed lines denote the core radius at 0.25 Mpc and the virial radius at 1.2 Mpc. Within the errors, there is no strong trend of the optical bar fraction with local environment density. The error bars show the statistical Poisson errors in each bin.
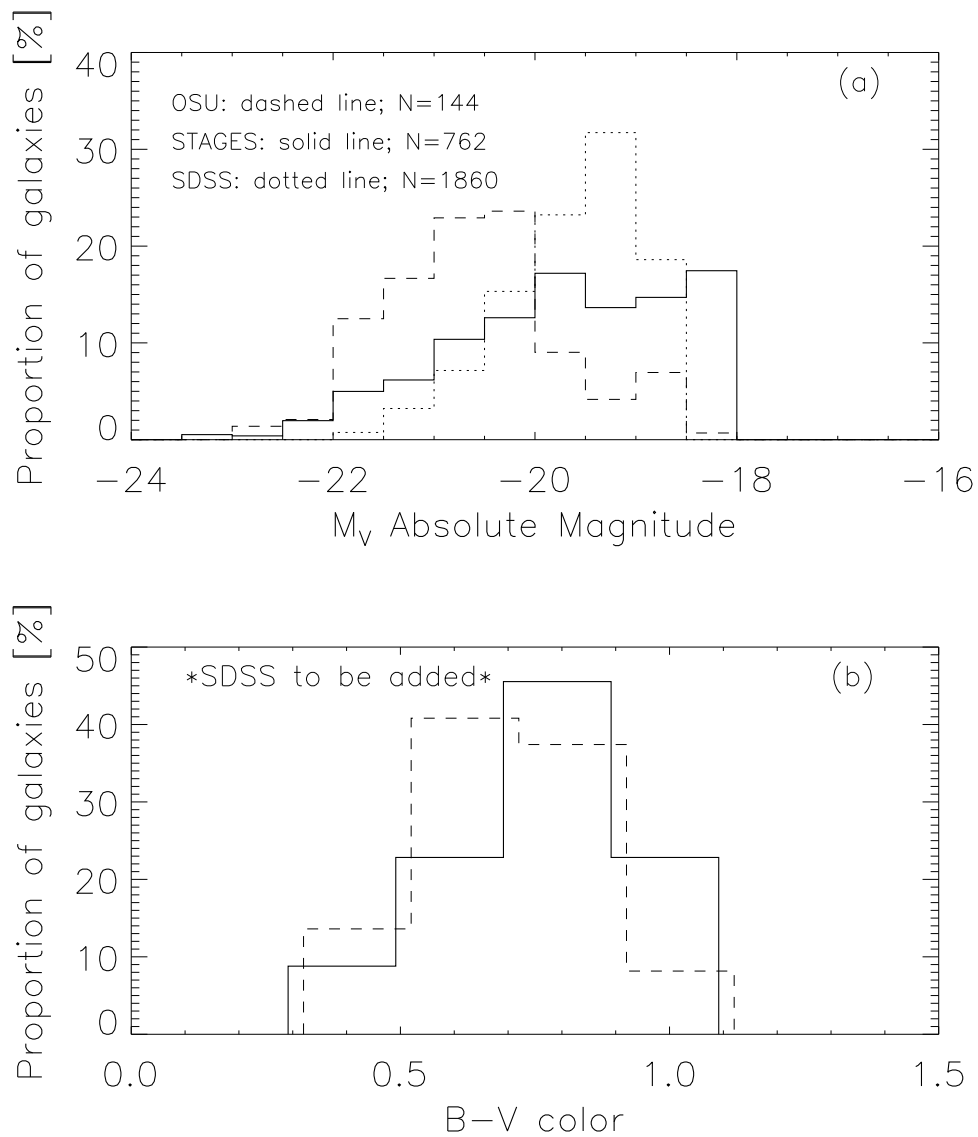
FIG. 13.— The absolute magnitude $M_{\rm V}$ (a) and rest-frame $U - V$ color (b) distributions are shown for the STAGES (solid line), OSUBSGS (dashed line), and SDSS (dotted line) samples. The OSUBSGS sample is brighter than both the SDSS and STAGES samples, and somewhat bluer than the STAGES sample. **U-V of SDSS to be added in panel b**
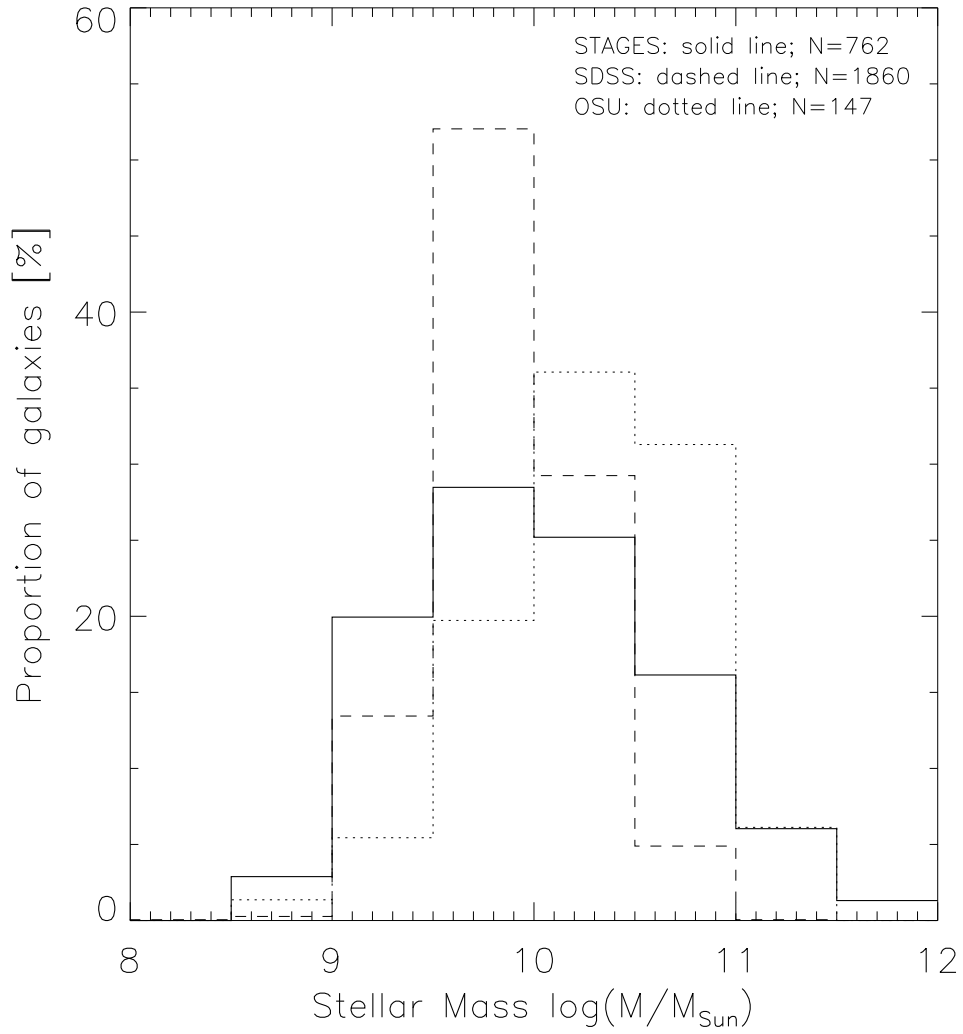
FIG. 14.— The stellar mass distribution of the OSU (dashed line), STAGES (solid line), and SDSS (dotted line) samples are over-plotted. The OSU and STAGES samples have similar range in stellar mass, however, the OSU sample is comprised of slightly more massive galaxies on average. The SDSS sample has a much narrower range in mass, with most galaxies lying between $M_*/M_\odot = 10^{9.5}$ and $10^{10.5}$
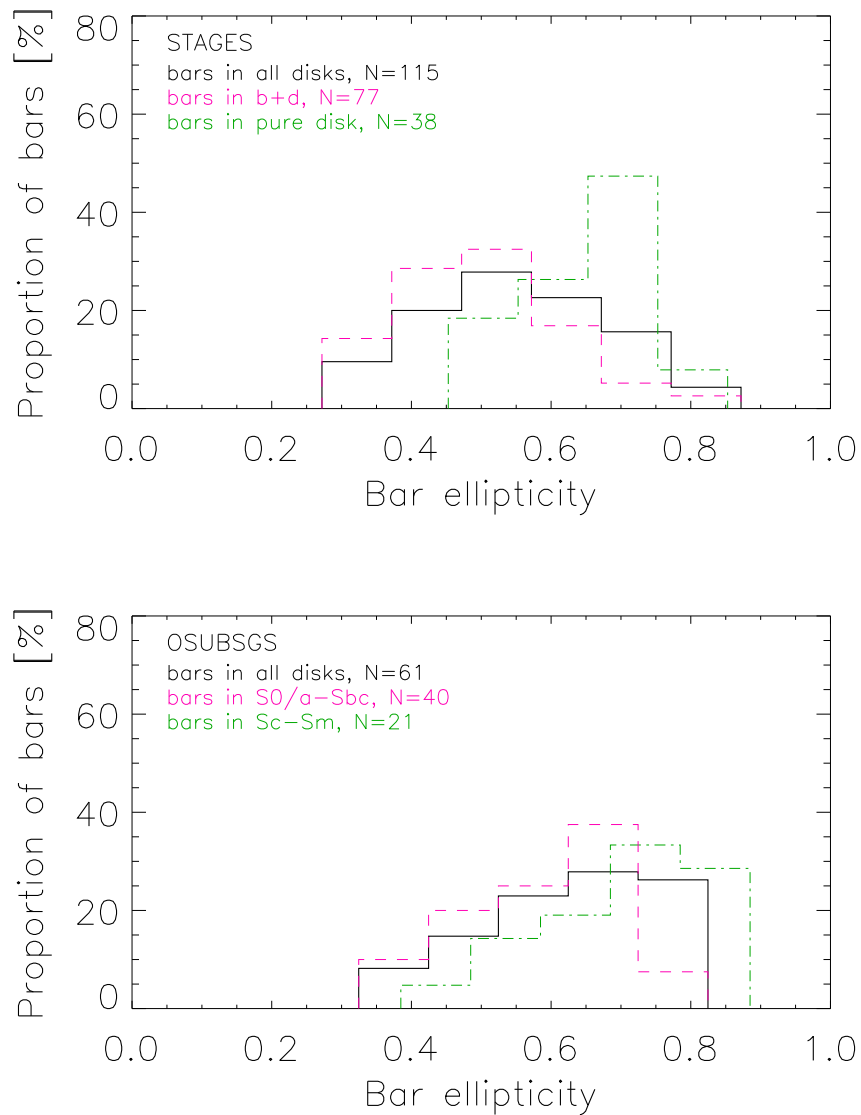
FIG. 15.— (a) Distribution of bar peak ellipticity e_{bar} for the STAGES sample. The solid black line shows the ellipticity distribution for all bars. The pink and green lines show the ellipticity distributions for bars in galaxies visually classified as 'bulge+disk' and 'pure disk', respectively. Bars in galaxies classified as 'bulge+disk' appear rounder than those in 'pure disk' galaxies. (b) Distribution of bar peak ellipticity e_{bar} for the OSUBSGS sample. The pink and green lines show the ellipticity distributions for bulge-dominated (S0-Sbc) and disk-dominated (Sc-Sm) galaxies, respectively. Again, bars in bulge-dominated galaxies appear rounder. In addition, bars in the STAGES supercluster sample appear weaker on average than those in the OSUBSGS sample. The result of lower e_{bar} in STAGES compared to OSU could be due to more bulge-dominated hosts in STAGES than OSU. This effect could be an artifact due to the dilution of the bar ellipticity by the bulge. It could also be an intrinsic effect.
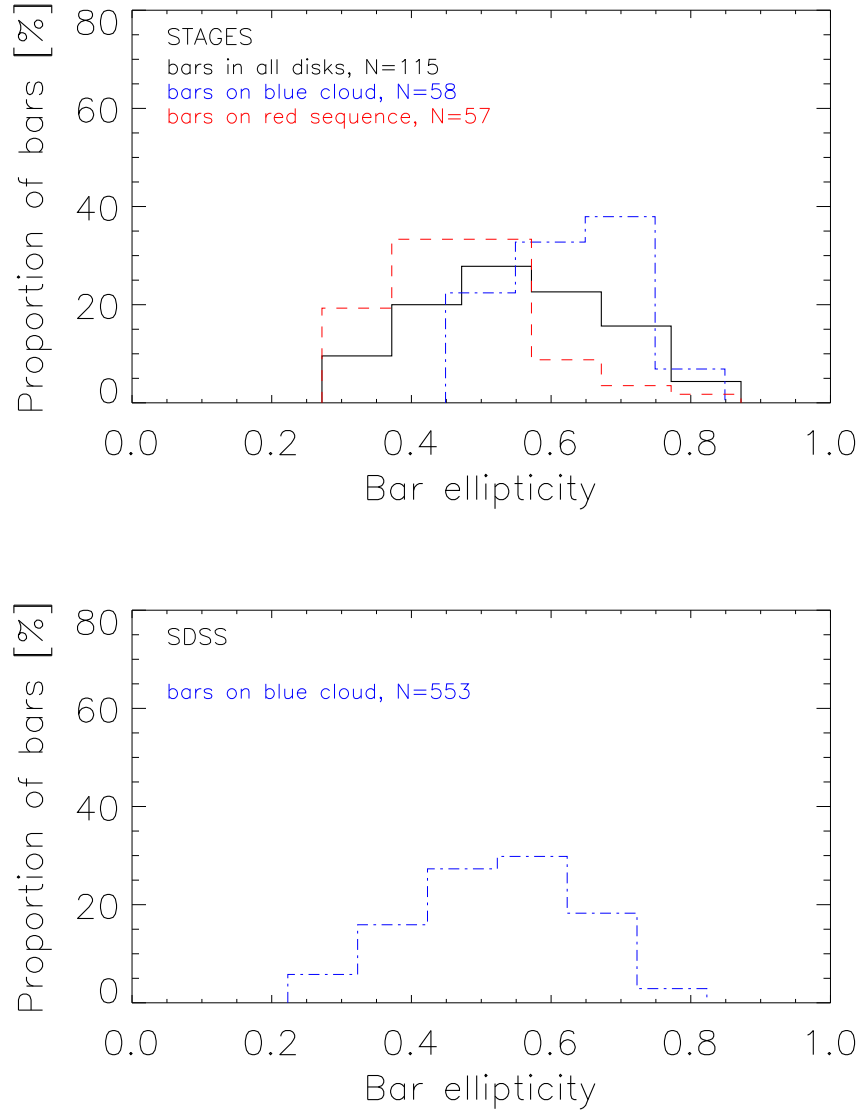
FIG. 16.— (a) e_{bar} distributions for the STAGES supercluster sample. The distributions are split to show the blue-cloud and red-sequence. It is evident that blue-cloud galaxies appear to host stronger bars than those on the red sequence. (b) e_{bar} distribution for the SDSS field sample. This sample is made up of only blue-cloud galaxies.
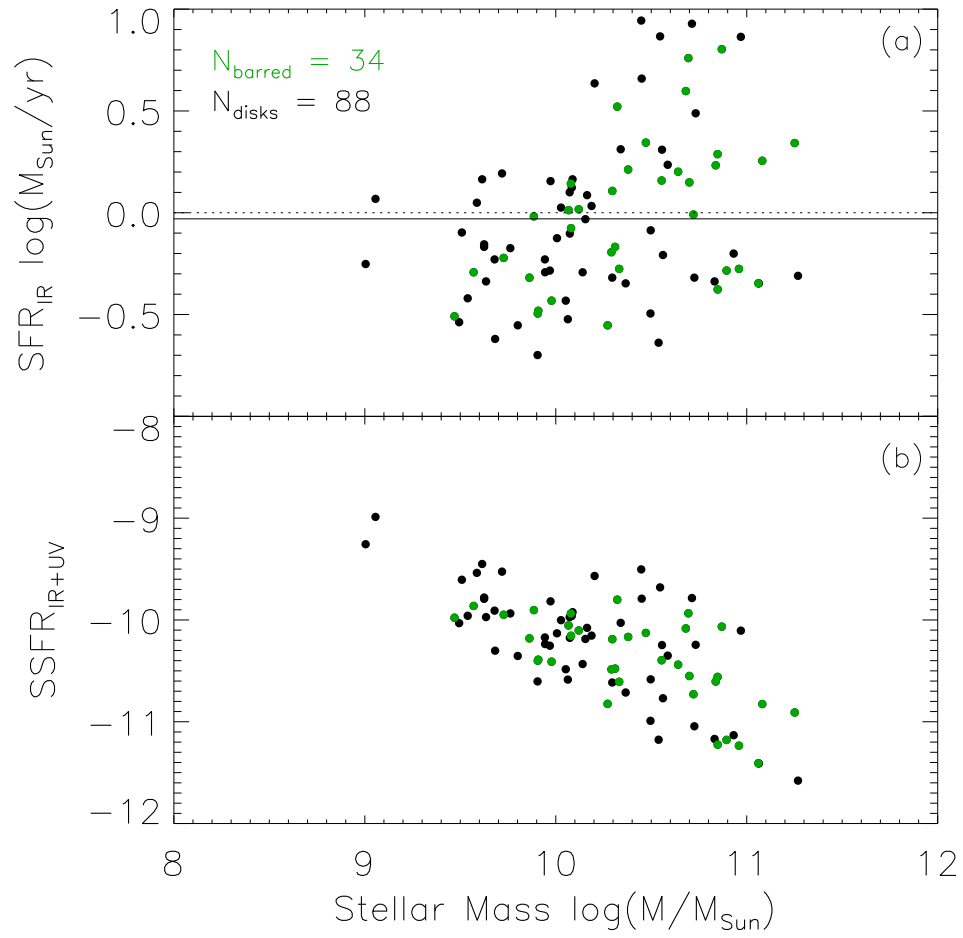
Fig. 17.— **under development**